Pseudodipolar interaction and antiferromagnetism in R_2CuO_4 compounds (R=Pr, Nd, Sm, and Eu)

D. Petitgrand
Laboratoire Léon Brillouin (CEA-CNRS), CE-Saclay, 91191 Gif-sur-Yvette, Cedex, France

S. V. Maleyev
Petersburg Nuclear Physics Institute, Gatchina, St. Petersburg 188350, Russia

Ph. Bourges
Laboratoire Léon Brillouin (CEA-CNRS), CE-Saclay, 91191 Gif-sur-Yvette, Cedex, France

A. S. Ivanov
Institut Laue-Langevin, Boîte Postale 156, F-38042 Grenoble Cedex 9, France and Russian Research Center ''Kurchatov Institute,'' 123182 Moscow, Russia

(Received 21 April 1998)

It is shown that pseudodipolar interaction allows one to explain static and dynamic properties of the noncollinear antiferromagnets, R_2CuO_4, in the temperature range where the rare-earth (RE) angular momenta are slightly polarized by the antiferromagnetic (AF) ordered Cu^{2+} spins. The spin-wave spectrum is determined and the inelastic neutron scattering cross section is evaluated taking into account interference related to the noncollinear arrangement of the copper spins in the adjacent CuO_2 planes. The detailed experimental data for low-energy inelastic neutron scattering in Pr_2CuO_4 are presented. Two in-plane spin-wave branches are observed in accordance with the theoretical predictions. Parameters of the intraplane and interplane pseudodipolar interactions are determined. The former appears by one order of magnitude larger than the theoretically one predicted for an isolated CuO_2 plane. We confirm this result by the analysis of the elastic neutron scattering data in magnetic field. Comparison of the spin-wave neutron scattering in Pr_2CuO_4 and Nd_2CuO_4 published earlier reveals the strong dependence of the in-plane anisotropy on the type of the RE ion. General expression for the ground-state energy in magnetic field applied parallel to the CuO_2 planes is derived and analyzed. It is shown that the spin-flop transition is of second order if the field is applied along the [1,1,0] direction. [S0163-1829(98)02746-5]

I. INTRODUCTION

During last decade magnetic properties of dielectric cuprates, which are parent compounds for the high-T_c superconductors were extensively investigated. In particular, compounds R_2CuO_4 (R=Pr, Nd, Sm, and Eu) were studied.[1–5] In these materials as well as in other insulating cuprates La_2CuO_4 and $YBa_2Cu_3O_{6+x}$ ($x \leqslant 0.4$) the long-range three-dimensional (3D) antiferromagnetic order stabilizes below $T_N \sim 250-410$ K due to very strong in-plane exchange interaction between Cu^{2+} $S=1/2$ spins and weak interplane coupling. The easy-plane anisotropy retains spins within CuO_2 planes. However some structural peculiarities distinguish the R_2CuO_4 family as well as $Sr_2CuO_2Cl_2$ (Refs. 6 and 7 from other antiferromagnetic cuprates. For the following it is important that R_2CuO_4 materials have a tetragonal structure where Cu^{2+} ions form a body-centered lattice [see Fig. 1(a)]. As a result in the antiferromagnetic state Cu^{2+} ions in the adjacent CuO_2 planes do not interact in the mean-field approximation if one assumes conventional isotropic exchange coupling. Therefore some weak interactions may manifest themselves, which are masked in other cuprates. This suggestion is confirmed by noncollinearity of the magnetic structure revealed by the neutron scattering in magnetic field[1–5] [see Fig. 1(b)]. In Refs. 1 and 8 the noncollinearity has been attributed to the biquadratic exchange. However, this exchange gives equal contributions to the ground-state energy of both structures shown in Fig. 1(b). Hence, it should be some other interaction which distinguish them. We suggest that it is the pseudodipolar (PD) interaction.

The magnetic moments of rare earth (RE) ions is the second peculiarity of the R_2CuO_4 family. Recently it has been thoroughly reviewed in Ref. 9, where it was shown that magnetic properties of the material strongly depends on the type of RE ion. In the case of Pr_2CuO_4 the Pr^{3+} ions have a nonmagnetic singlet ground state and the first excited state is a doublet at 18 meV.[1] Hence well below the Néel temperature $T_N \simeq 280$ K the Pr^{3+} momenta are slightly polarized due to the interaction with Cu^{2+} ordered spins and remain inactivated thermally.[1] As a result at low T they give some temperature independent contribution to the effective Cu-Cu interaction.

The ground states of Nd^{3+} and Sm^{3+} ions are Kramers doublets that are split slightly due to interaction with copper spins. For Nd_2CuO_4, the Nd spin excitation spectrum is ranged between 0.1 and 0.8 meV (Refs. 16 and 17) and that would correspond to a characteristic splitting, $\delta \sim 3.0$ K.[9] Neglecting this splitting one has the single-ion susceptibility

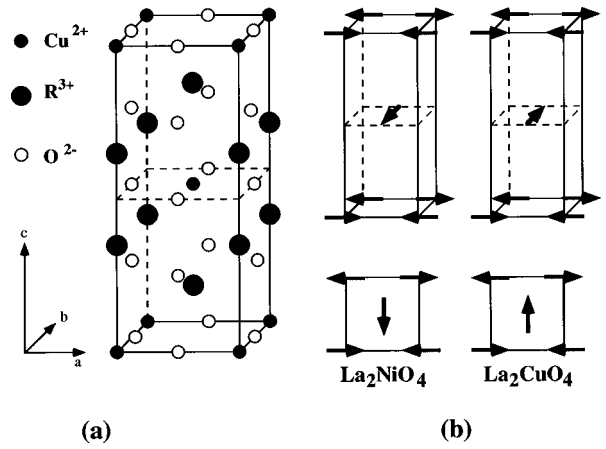

FIG. 1. (a) Crystallographic structure of the tetragonal compounds R_2CuO_4 (R=Pr, Nd, Sm, and Eu); Cu ions form a body-centered tetragonal lattice. (b) Two observed noncollinear magnetic structures: I (La_2NiO_4 type) left; Pr, Nd (I,III), Sm and II (La_2CuO_4 type) right; Eu, Nd (II) and their projections on the basal plane. For Nd_2CuO_4 phases I, II, and III are observed at $T_N \simeq 250$ K$>T>80$ K, 80 K$>T>30$ K, and 30 K$>T$, respectively.

in the form $\chi = C/T$. In the case of Nd_2CuO_4, this susceptibility is likely responsible for the two spin reorientational transitions at $T_1 \simeq 80$ K and $T_2 \simeq 30$ K (Refs. 9 and 10) (see Sec. IX). In the case of Sm_2CuO_4 there is some additional transition at 20 and that awaits further investigation.[4,9] Eu_2CuO_4 is the last member of the considered family with noncollinear spin structure. The Eu^{3+} ion has $J=0$ and do not contribute to the low-temperature magnetism of the compound. Unfortunately, there is a structural phase transition at $T=140$ K (Refs. 11 and 12) [of lower symmetry identical to that observed in Gd_2CuO_4 (Ref. 13) and the spin ordering below it has not been yet fully determined.

This paper is devoted to the low-temperature properties of the Cu subsystem in the temperature range, where RE momenta are slightly polarized by the interaction with Cu^{2+} spins. We assume that in this temperature range the influence of the RE ions on the Cu^{2+} spins may be properly taken into account by renormalization of the constants of the weak Cu-Cu interactions such as the easy-plane anisotropy and parameters of the pseudodipolar Hamiltonian. Hence, for Pr_2CuO_4 our theoretical consideration should be applicable in the whole temperature range well below $T_N \simeq 280$ K with temperature-independent parameters. In the case of Nd_2CuO_4 it holds at $T \gg 3$ K (Ref. 9) and according to Ref. 14 the parameters strongly depend on T (see Secs. VI and IX). For Sm_2CuO_4 the temperature range of the theory is restricted by $T>20$ K. The theory is hardly applicable to Eu_2CuO_4 due to the above-mentioned phase transition at $T=140$ K. We note also that low-temperature spin waves in Nd subsystem below 1.5 K has been studied recently in Refs. 9 and 15–17. There is also low-energy ($\omega \lesssim 2$ MeV) quasielastic scattering on the Nd subsystem[18] but we do not consider it.

The noncollinearity may be easily explained if one assumes the dependence of the interaction on the direction of the bonds connecting two Cu^{2+} spins (see below, Sec. II and Ref. 9). This interaction may be represented as the pseudodipolar (PD) one proposed by Van Vleck in 1937,

$$V_{pd} = \tfrac{1}{2} \sum_{\ell\ell'} V(\mathbf{R}_{\ell\ell'})(\mathbf{S}_{\ell'}\hat{\mathbf{R}}_{\ell\ell'})(\mathbf{S}_{\ell}\hat{\mathbf{R}}_{\ell\ell'}), \qquad (1)$$

where ℓ and ℓ' label the lattice sites and the function $V(R)$ decreases faster than R^{-3} as $R \to \infty$.

The PD interaction between Cu^{2+} and Nd^{3+} ions has been first considered in Refs. 19. Recently it has been used for the complete description of the spin structure of the R_2CuO_4 family.[9] In particular, it has been shown that it is responsible for the noncollinear structure of Cu as well as of RE subsystems. It was used also for an explanation of weak ferromagnetism of the tetragonal compound $SrCu_3O_4Cl_2$.[20] Microscopic derivation of the PD interaction between Cu spins in CuO_2 planes has been done in Refs. 21–23 in the frame of the Hubbard model using on-site Coulomb exchange and spin-orbit interactions. It should be noted also that the PD interaction appears in metals as a result of the skew scattering[24] that is a consequence of the ordinary exchange interaction between ions with $L \neq 0$ and conducting band.[25] The result may be easily generalized for interaction of d and f electrons via oxygen $2p$ orbitals.[26] The PD interaction has been used also for explanation spin-wave dispersion in metallic Pr.[27]

In this paper we develop spin-wave theory for the noncollinear cuprates above RE ordering temperature taking into account both interplane and intraplane pseudodipolar interactions. We demonstrate that the former splits the in-plane spin-wave spectrum into acoustic and optical branches whereas the latter (intraplane PD interaction) gives rise to the fourfold (square) anisotropy.[21,22] As a result the in-plane spin wave gap appears due to the interaction between spin-waves. This gap has been obtained in Ref. 22 using a phenomenological Hamiltonian. We confirm this result by microscopic calculations and determine its dependence on the sublattice orientation in the (a,b) plane. This dependence is essential for determination of the spin configuration in magnetic field.

Next, we present detailed neutron scattering data in Pr_2CuO_4. We observed acoustic and optical spin-wave branches and determined the in-plane and out-of-plane spin-wave gaps. We demonstrated a destructive interference in the neutron scattering on the acoustic branch, which is a consequence of the noncollinear spin structure and the PD interaction between adjacent CuO_2 planes. From these data we determine the parameters of the PD interaction. In particular, the intraplane PD interaction appears to be by one order of magnitude larger than calculated in Refs. 22 and 23. Comparing this result with the strong T dependence of the gaps in Nd_2CuO_4 observed previously[14] we conclude that along with the PD interaction and anisotropic exchange considered in Refs. 22 and 23 there is an additional contribution to the square and uniaxial anisotropies connected with the RE ions.

The spin orientation in magnetic field, experimentally studied in Refs. 1–5 is the next problem considered in the paper. We derive the ground-state energy, which governs this orientation for the magnetic field arbitrarily directed in the CuO_2 planes. In particular, we show that if the field is along the [1,1,0] direction the spin-flop transition is of second order and the following relation holds

$$g\mu H_c=\Delta_0, \tag{2}$$

where H_c is the critical field of the transition and Δ_0 is the in-plane spin-wave gap at $H=0$. Using this equation we analyze the data of Ref. 1 and confirm the large value of Δ_0 obtained in our inelastic scattering experiments. The spin-wave spectrum in magnetic field is considered too. We show that one of the branches becomes gapless at the spin-flop transition.

Analysis of the ground-state energy in magnetic field reveals a new phenomenon: Bose condensation of the uniform spin waves in magnetic field canted to the sublattice magnetization. Related crossover of the sublattice orientation as function of H near the spin-flop transition was observed recently in Pr_2CuO_4.[28]

This paper is organized in the following way. In Sec. II we formulate the model used below. Section III is devoted to the linear spin-wave theory. The intraplane anisotropy and in-plane spin-wave gap is considered in Section IV. In this section we present also expressions for the spin-wave branches along the magnetic rod. Theoretical expressions for the neutron scattering cross sections are derived in Sec. V. Inelastic neutron scattering data on Pr_2CuO_4 are presented in Sec. VI, where we also discuss them as well as corresponding data for Nd_2CuO_4.[14] Section VII is devoted to consideration of the spin configuration of the noncollinear antiferromagnets in magnetic field arbitrarily directed in the basal plane. The spin-wave spectrum in magnetic field and inelastic neutron scattering is considered in Sec. VIII. In the last section we summarize principal results of the paper and give additional comments for some of them. In Appendix A we derive the expression for the ground state energy in magnetic field. The Green's functions in magnetic field are calculated in Appendix B.

II. MODEL

We represent the Hamiltonian of the Cu^{2+} spin system in the following form:

$$H=H_{ex}+H_A+H_{PD}+g\mu\mathbf{H}\sum_{n\ell}\mathbf{S}_\ell, \tag{3}$$

where H_{ex} is the isotropic exchange interaction, H_A is the uniaxial anisotropy, H_{PD} is the pseudodipolar interaction, and the last term is the interaction with external magnetic field and $g\mu>0$.

Below we consider the interaction between the nearest neighbors only. In this case H_{ex} can be written as

$$H_{ex}=\tfrac{1}{2}\sum_{\ell,\ell',n}J_{\ell\ell'}\mathbf{S}_{\ell n}\mathbf{S}_{\ell' n}-\tfrac{1}{2}\sum_{\ell nn'}I_{nn'}\mathbf{S}_{\ell n}\mathbf{S}_{\ell n'}+\tfrac{1}{2}\sum_{\ell,\ell_1,n}M_{\ell\ell_1}\mathbf{S}_{\ell n}\mathbf{S}_{\ell_1 n}, \tag{4}$$

where ℓ and ℓ' denote sites in CuO_2 planes and n enumerates planes; $J_{\ell\ell'}$, $I_{nn'}$, and $M_{\ell\ell_1}$ are the nearest-neighbor exchange interactions within CuO_2 planes, along the c axis and between Cu^{2+} ions in the adjacent planes, respectively. In particular, the index ℓ_1 in the last term of Eq. (4) is equal to $\ell+(\pm a,\pm b,\pm c)/2$.

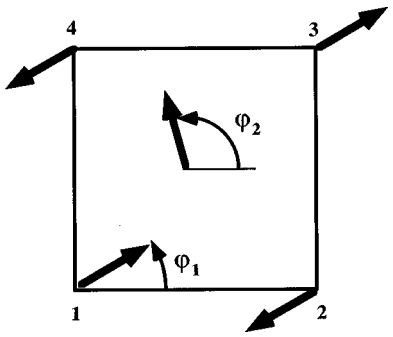

FIG. 2. Ground-state antiferromagnetic spin configuration in the unit cell of R_2CuO_4. The spin orientation in the adjacent layers are given by angles φ_1 and φ_2.

The uniaxial anisotropy in Eq. (3) we consider as a part of the anisotropic exchange and represent it as

$$H_A=-\tfrac{1}{2}\sum_{\ell,\ell',n}A_{\ell\ell'}S^c_{\ell n}S^c_{\ell' n} \tag{5}$$

and the easy-plane anisotropy takes place if $A_{\ell\ell'}>0$.

It is convenient to divide the PD interaction into interplane and intraplane parts. For the former we have

$$H_I=\tfrac{1}{2}\sum_{\ell,\ell_1,n}Q_{\ell\ell_1}(\mathbf{S}_{\ell n}\hat{\mathbf{R}}_{\ell\ell_1})(\mathbf{S}_{\ell_1 n}\hat{\mathbf{R}}_{\ell\ell_1}), \tag{6}$$

where $\hat{\mathbf{R}}_{\ell\ell_1}=\mathbf{R}_{\ell\ell_1}/R_{\ell\ell_1}$. Slightly modifying Eq. (1) we represent the intraplane PD interaction in the traceless form as in Refs. 21–23:

$$H_P=\tfrac{1}{2}\sum_{\ell,\ell'}P_{\ell\ell'}[(\mathbf{S}_\ell\hat{\mathbf{R}}_{\ell\ell'})(\mathbf{S}_{\ell'}\hat{\mathbf{R}}_{\ell\ell'})-\tfrac{1}{2}(S^a_\ell S^a_{\ell'}+S^b_\ell S^b_{\ell'})], \tag{7}$$

where a and b are coordinate axes in CuO_2 plane [see Fig. 1(a)]. The interaction (7) may be represented in the form (1) with corresponding change of both interactions $J_{\ell\ell'}$ and $A_{\ell\ell'}$.

Interplane PD interaction (6) explains the observed spin structure.[19] Indeed, let us consider in the mean-field approximation interaction between the central spin and corner spins shown in Fig. 2. Simple calculations get

$$E_i=4S^2Q_0\sin(\varphi_1+\varphi_2),\qquad Q_0=Q\frac{a^2}{2a^2+c^2}, \tag{8}$$

where Q is the nearest-neighbor interplane PD interaction and angles φ_1 and φ_2 are shown in Fig. 2. This energy is minimal if $\varphi_1+\varphi_2=-(\pi/2)\mathrm{sgn}Q_0$. In this case the noncollinear ordering is fixed by the intraplane square anisotropy which appears as a result of zero-point contribution to the ground-state energy (Refs. 21 and 22 and below in Sec. IV). It should be noted also that the interplane PD interaction leads to ferromagnetic ordering of the neighboring spins along the c axis shown in Fig. 1(b) because the interactions of the central spin with lower and upper planes have the form given by Eq. (8). Hence, we do not need any further ferro-

magnetic exchange between copper spins along $\hat{c}$ axis given by the second term in Eq. (4) and, actually, the observed spin-wave spectrum does not reveal this interaction (see Sec. VI).

We divide the whole system of CuO_2 planes in two subsystems 1, and 2, which include the corner and central Cu^{2+} ions in Figs. 1(a) and 1(b), respectively. They are connected by the vector $\boldsymbol{\delta}=(a,b,c)/2$. In every subsystem Cu^{2+} spins are arranged antiferromagnetically in planes and ferromagnetically along the c axis. For the in-plane spin orientation we assign angles φ_1 and φ_2 for the first and the second subsystems, respectively as shown in Fig. 2.

The whole spin system may be considered now as consisting of four sublattices and needing four sets of the spin operators. It is quite inconvenient. So we, rather, use another type of description involving one set of spin operators per subsystem and the antiferromagnetic (AF) propagating vector $\mathbf{k}_0$ for which we have two equivalent forms:

$$\mathbf{k}_0^{(1)}=\frac{\pi}{a}(1,1,0), \quad \mathbf{k}_0^{(2)}=\frac{\pi}{a}(-1,1,0). \tag{9}$$

We will set below $\mathbf{k}_0=\mathbf{k}_0^{(2)}$; in this case we have $\exp(i\mathbf{k}_0\boldsymbol{\delta})=1$. In each system of planes the spins may be represented in the following form:

$$\mathbf{S}_{\ell m}^{(\lambda)}=(\mathbf{S}_{\ell mz}^{(\lambda)}\hat{e}_{z\lambda}+S_{\ell my}^{(\lambda)}\hat{e}_{y\lambda})e^{i\mathbf{k}_0\mathbf{R}_{\ell}^{(\lambda)}}+S_{\ell mx}^{(\lambda)}\hat{c}, \tag{10}$$

where $\lambda=1,2$; $\mathbf{R}_{\ell}^{(1)}=\mathbf{R}_{\ell}$, $\mathbf{R}_{\ell}^{(2)}=\mathbf{R}_{\ell}+\boldsymbol{\delta}$, ℓ and m enumerate unit cells in (a,b) planes and along the c axis, respectively, and

$$\begin{aligned}\hat{e}_{z\lambda}&=(\cos\varphi_\lambda,\sin\varphi_\lambda,0),\\ \hat{e}_{y\lambda}&=(-\sin\varphi_\lambda,\cos\varphi_\lambda,0),\\ \hat{c}&=(0,0,1),\end{aligned} \tag{11}$$

where $z1$ and $z2$ are directions at the sublattice magnetization for subsystems 1 and 2. Vector $\mathbf{k}_0$ and unit vectors $\hat{e}_{z\lambda}$, $\hat{e}_{y\lambda}$, and $\hat{c}$ determine the frame of reference for the components of the spin operators. Below we will use for them the well-known representation

$$\begin{aligned}S_{\ell mz}^{(\lambda)}&=S-a_{\ell m\lambda}^{+}a_{\ell m\lambda},\\ S_{\ell m\lambda}^{+}=S_{\ell m\lambda}^{(c)}+iS_{\ell m\lambda}^{(y)}&=\sqrt{2S}(a_{\ell m\lambda}-a_{\ell m\lambda}^{+}a_{\ell m\lambda}^{2}/2S),\\ S_{\ell m\lambda}^{-}=S_{\ell m\lambda}^{(c)}-iS_{\ell m\lambda}^{(y)}&=\sqrt{2S}a_{\ell m\lambda}^{+}.\end{aligned} \tag{12}$$

Now we rewrite Eqs. (4)–(7) in momentum space,

$$H_{ex}=\tfrac{1}{2}\sum_{\mathbf{k}}(J_{\mathbf{k}}-I_{\mathbf{k}})(\mathbf{S}_{\mathbf{k}1}\mathbf{S}_{-\mathbf{k}1}+\mathbf{S}_{\mathbf{k}2}\mathbf{S}_{-\mathbf{k}2})+\sum_{\mathbf{k}}M_{\mathbf{k}}\mathbf{S}_{\mathbf{k}1}\mathbf{S}_{-\mathbf{k}2}, \tag{13}$$

$$H_A=-\tfrac{1}{2}\sum_{\mathbf{k}}A_{\mathbf{k}}(S_{\mathbf{k}1}^{c}S_{-\mathbf{k}1}^{c}+S_{\mathbf{k}2}^{c}S_{-\mathbf{k}2}^{c}), \tag{14}$$

$$H_I=\sum_{\mathbf{k},\alpha,\beta}Q_{\mathbf{k}}^{\alpha\beta}S_{\mathbf{k}1}^{\alpha}S_{-\mathbf{k}2}^{\beta}, \tag{15}$$

$$\begin{aligned}H_P=\frac{P}{2}\sum_{\mathbf{k}}&(\cos k_a-\cos k_b)\\ &\times(S_{\mathbf{k}1}^{a}S_{-\mathbf{k}1}^{a}+S_{\mathbf{k}2}^{a}S_{-\mathbf{k}2}^{a}-S_{\mathbf{k}1}^{b}S_{-\mathbf{k}1}^{b}-S_{\mathbf{k}2}^{b}S_{-\mathbf{k}2}^{b}),\end{aligned} \tag{16}$$

where P is the nearest-neighbor intraplane PD interaction and we define the Fourier transform as

$$\mathbf{S}_{\mathbf{k}\lambda}=N^{-1/2}\sum_{\ell m}\mathbf{S}_{\ell m\lambda}\exp(-i\mathbf{k}\mathbf{R}_{\ell m}) \tag{17}$$

and similar expressions for the operators $a_{\ell m\lambda}$ and $a_{\ell m\lambda}^{+}$.

Here N is the total number of unit cells and

$$\begin{aligned}J_{\mathbf{k}}&=2J(\cos k_a+\cos k_b),\\ I_{\mathbf{k}}&=2I\cos k_c,\\ A_{\mathbf{k}}&=2A(\cos k_a+\cos k_b),\\ M_{\mathbf{k}}&=8M\cos\frac{k_a}{2}\cos\frac{k_b}{2}\cos\frac{k_c}{2},\end{aligned} \tag{18}$$

where $k_a=k^{(a)}a$, etc. and $J_0=4J$. For components of the symmetrical tensor $Q_{\alpha\beta}$ we have

$$\begin{aligned}Q_{\mathbf{k}}^{aa}=Q_{\mathbf{k}}^{bb}=u^2Q_{\mathbf{k}}^{cc}&=8Q_0\cos\frac{k_a}{2}\cos\frac{k_b}{2}\cos\frac{k_c}{2},\\ Q_{\mathbf{k}}^{ab}&=-8Q_0\sin\frac{k_a}{2}\sin\frac{k_b}{2}\cos\frac{k_c}{2},\\ Q_{\mathbf{k}}^{ac}&=-8\frac{Q_0}{u}\sin\frac{k_a}{2}\cos\frac{k_b}{2}\sin\frac{k_c}{2},\\ Q_{\mathbf{k}}^{bc}&=-8\frac{Q_0}{u}\cos\frac{k_a}{2}\sin\frac{k_b}{2}\sin\frac{k_c}{2},\end{aligned} \tag{19}$$

where $u=a/c$ and $Q_0=a^2Q/(2a^2+c^2)$. Diagonal components of $Q^{\alpha\beta}$ renormalize interplane exchange M and give rise to small additional uniaxial anisotropy that may be neglected. The nondiagonal components $Q_{\mathbf{k}}^{ac}$ and $Q_{\mathbf{k}}^{bc}$ are zero at the magnetic rods where $k_{a,b}=0$ or $k_{a,b}=\pm\pi/a$; the only lines near which the PD interaction may be important, because in other parts of the $\mathbf{k}$ space it is negligible comparing with the strong intraplane exchange coupling. Thus below we will take into account the nondiagonal $Q_{\mathbf{k}}^{ab}$ component only.

III. LINEAR SPIN-WAVE THEORY

In this section we present results of the linear spin-wave theory in zero magnetic field. For an isolated plane, they coincide with results of Refs. 21 and 22. However, we rewrite them in a form convenient for the further consideration of the spin-wave interaction. The interplane PD coupling splits the spin-wave spectrum into acoustic and optical branches that are observed experimentally. Corresponding results are presented in Sec. VI.

Using Eqs. (12)–(17) and neglecting higher-order terms we obtain the spin-wave Hamiltonian consisting of zero-

order, linear and bilinear terms. The zero-order term gives the classical ground-state energy. Its part depending on the spin orientations has the form

$$\Delta E_{12}=NS^2Q^{ab}_{\mathbf{k_0}}\sin(\varphi_1+\varphi_2)=8NS^2Q_0\sin(\varphi_1+\varphi_2). \tag{20}$$

Here we have taken into account our choice of $\mathbf{k}_0=\mathbf{k}_0^{(2)}$.

The equilibrium spin configuration is determined by the minimum of this expression,[19] if one neglects other φ-depended contributions to the ground state energy (see below Secs. IV and VI). It should be noted also that Eq. (20) determines the spin configuration regardless of choices of $\mathbf{k}_0$ given by Eq. (9). Indeed, according to Eq. (10) the definition of the frame of reference for the adjacent plane contains a factor $\exp(i\mathbf{k}_0\boldsymbol{\delta})$, which is equal to -1 and $+1$ for $\mathbf{k}_0=\mathbf{k}_0^{(1)}$ and $\mathbf{k}_0=\mathbf{k}_0^{(2)}$, respectively. In the first case we have an additional rotation on angle π which should be compensated by the replacement $\varphi_2\rightarrow\varphi_2+\pi$.

The linear term of the Hamiltonian is given by

$$W_1=\left[iSQ_{\mathbf{k}_0}\left(\frac{NS}{2}\right)^{1/2}\right]\cos(\varphi_1+\varphi_2)(a^+_{01}-a_{01}+a^+_{02}-a_{02}). \tag{21}$$

It should be eliminated in the same way as the linear terms related in presence of a magnetic field **H** (see Appendix A). However at $\mathbf{H}=0$ as well as at **H** along the [1,1,0] direction we have $\varphi_1+\varphi_2=\pm\pi/2$ and $W_1=0$ (see Sec. VI). The same holds if $H\|[1,0,0]$ below the spin-flop transition (see Sec. VII).

The bilinear spin-wave Hamiltonian may be represented as follows:

$$H_{SW}=H_1+H_2+V,$$

$$H_\lambda=\sum_{\mathbf{k}}\ [E_{\mathbf{k},\lambda}a^+_{\mathbf{k},\lambda}a_{\mathbf{k},\lambda}+\tfrac{1}{2}B_{\mathbf{k},\lambda}(a^+_{\mathbf{k},\lambda}a^+_{-\mathbf{k}\lambda}+a_{\mathbf{k},\lambda}a_{-\mathbf{k},\lambda})], \tag{22}$$

$$V=\sum_{\mathbf{k}}\ [C_{\mathbf{k}}(a^+_{\mathbf{k},1}a_{\mathbf{k},2}+a^+_{\mathbf{k},2}a_{\mathbf{k},1})+D_{\mathbf{k}}(a^+_{\mathbf{k},1}a^+_{-\mathbf{k},2}+a_{\mathbf{k},1}a_{-\mathbf{k},2})],$$

where $\lambda=1,2$ and if $\mathbf{H}=0$, it gives

$$\begin{aligned}E_{\mathbf{k}\lambda}&=S(J_0+I_0-I_{\mathbf{k}}-\tfrac{1}{2}A_{\mathbf{k}}+\tfrac{1}{2}\gamma_{\mathbf{k}}\cos 2\varphi_\lambda)+R_0,\\ B_{\mathbf{k}\lambda}&=S(J_{\mathbf{k}}-\tfrac{1}{2}A_{\mathbf{k}}-\tfrac{1}{2}\gamma_{\mathbf{k}}\cos 2\varphi_\lambda),\end{aligned} \tag{23}$$

where

$$\begin{aligned}\gamma_{\mathbf{k}}&=P(\cos k_a-\cos k_b),\\ R_0&=-SQ^{ab}_{\mathbf{k_0}}\sin(\varphi_1+\varphi_2)=-8SQ_0\sin(\varphi_1+\varphi_2)>0,\end{aligned} \tag{24}$$

and

$$\begin{aligned}C_{\mathbf{k}}&=\tfrac{1}{2}S[M_{\mathbf{k}}+M_{\mathbf{k}+\mathbf{k}_0}\cos(\varphi_1-\varphi_2)-Q^{ab}_{\mathbf{k}+\mathbf{k}_0}\sin(\varphi_1+\varphi_2)],\\ D_{\mathbf{k}}&=\tfrac{1}{2}S[M_{\mathbf{k}}-M_{\mathbf{k}+\mathbf{k}_0}\cos(\varphi_1-\varphi_2)+Q^{ab}_{\mathbf{k}+\mathbf{k}_0}\sin(\varphi_1+\varphi_2)].\end{aligned} \tag{25}$$

In Eqs. (22), the terms that contain $Q^{ac}_{\mathbf{k}}$ and $Q^{bc}_{\mathbf{k}}$ are omitted because on the magnetic rod we have $Q^{ac}=Q^{bc}=0$.

It is well known that all observable quantities may be evaluated using corresponding Green's functions determined as

$$G_{AB}(\omega)=-i\int_0^\infty dt\, e^{i\omega t}\langle[A(t),B(0)]\rangle. \tag{26}$$

They satisfy equations of motion,

$$\omega G_{AB}(\omega)+G_{[H,A],B}(\omega)=\langle[A,B]\rangle. \tag{27}$$

We will use below the following Green's functions:

$$\begin{aligned}G_{\lambda'\lambda}&=G_{a_{\lambda'},a^+_\lambda},\quad F^+_{\lambda'\lambda}=G_{a^+_{\lambda'},a^+_\lambda};\\ G^+_{\lambda'\lambda}&=G_{a^+_{\lambda'},a_\lambda};\quad F_{\lambda'\lambda}=G_{a_{\lambda'},a_\lambda}.\end{aligned} \tag{28}$$

Using these definitions and Eqs. (22) and (27) we get

$$\begin{aligned}(\omega-E_1)G_{11}-B_1F^+_{11}-CG_{21}-DF^+_{21}&=1,\\ B_1G_{11}+(\omega+E_1)F^+_{11}+DG_{21}+CF^+_{21}&=0,\\ -CG_{11}-DF^+_{11}+(\omega-E_2)G_{21}-B_2F^+_{21}&=0,\\ DG_{11}+CF^+_{11}+B_2G_{21}+(\omega+E_2)F^+_{21}&=0,\end{aligned} \tag{29}$$

where we omit the subscript **k**. Solution of these equations has the following form:

$$\begin{aligned}G_{11}&=[(\omega+E_1)(\omega^2-E_2^2+B_2^2)+(D^2-C^2)\omega\\ &\quad+(D^2+C^2)E_2-2B_2CD]\Delta^{-1},\\ F^+_{11}&=-[B_1(\omega^2-E_2^2+B_2^2)-B_2(C^2+D^2)+2CDE_2]\Delta^{-1},\end{aligned} \tag{30}$$

$$\begin{aligned}G_{21}&=[(\omega+E_1)(\omega+E_2)C-B_1D(\omega+E_2)-B_2D(\omega+E_1)\\ &\quad+B_1B_2C+CD^2-C^3]\Delta^{-1},\\ F^+_{21}&=-[(\omega+E_1)(\omega-E_2)D-B_1C(\omega-E_2)\\ &\quad+(\omega+E_1)B_2C-B_1B_2D+D^3-C^2D]\Delta^{-1},\end{aligned}$$

where

$$\begin{aligned}\Delta(\omega)&=(\omega^2-E_1^2+B_1^2)(\omega^2-E_2^2+B_2^2)\\ &\quad-2\omega^2(C^2-D^2)-2(E_1E_2+B_1B_2)(C^2+D^2)\\ &\quad+4(B_1E_2+B_2E_1)CD+(C^2-D^2)^2.\end{aligned} \tag{31}$$

The interaction between subsystems is very weak, and in this expression we should retain the terms containing C and D only if these quantities are multiplied by the large factor $SJ_{\mathbf{k}}$. Hence, we have to omit the second and last terms in Eq. (31). The solution of the equation $\Delta(\omega)=0$ determines the spin-wave spectrum and may be represented as follows:

$$\begin{aligned}\epsilon^2_\pm&=\frac{1}{2}\{\epsilon_1^2+\epsilon_2^2\pm[(\epsilon_1^2-\epsilon_2^2)^2+8(E_1E_2+B_1B_2)(C^2+D^2)\\ &\quad-16(B_1E_2+B_2E_1)CD]^{1/2}\},\end{aligned} \tag{32}$$

where $\epsilon^2_{1,2}=E^2_{1,2}-B^2_{1,2}$.

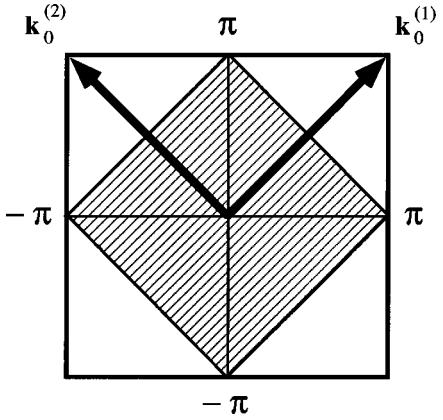

FIG. 3. Chemical Brillouin zone. The in-plane and out-of-plane spin waves correspond to hatched and unhatched parts of the zone, respectively. The former one coincides with the magnetic zone.

In the chosen convention, each subsystem is divided into two sublattices and the spin-wave spectrum consists of two branches known as in-plane and out-of-plane excitations. Interaction between subsystems 1 and 2 splits these excitations and we obtain four branches. Our expression (32) determines two branches only. It is a result of our approach based on the chemical cell instead of the magnetic one. The Brillouin zone is shown in Fig. 3 and its hatched part is the conventional magnetic zone. The in-plane and out-of-plane spin waves belong to hatched and unhatched parts of the Brillouin zone, respectively.

If we restrict the $\mathbf{k}$ space by the magnetic zone, the in-plane and out-of-plane spin waves will be determined by Eq. (32) as $\epsilon_{\mathbf{k}}^{(\pm)}$ and $\epsilon_{\mathbf{k}+\mathbf{k}_0}^{(\pm)}$ respectively. We then obtain four branches as expected. Neglecting the interaction between the two subsystems ($C=D=0, R_0=0$), we get

$$\epsilon_{\mathbf{k},1,2}^2 = S^2(J_0 - J_{\mathbf{k}} + I_0 - I_{\mathbf{k}} + \gamma_{\mathbf{k}} \cos 2\varphi_{1,2}) \times (J_0 + J_{\mathbf{k}} + I_0 - I_{\mathbf{k}} - A_{\mathbf{k}}), \tag{33}$$

where $\gamma_{\mathbf{k}}$ is given by Eq. (24). This expression may be rewritten as

$$\epsilon_{\mathbf{k},in\ 1,2}^2 = S^2(J_0 - J_{\mathbf{k}} + I_0 - I_{\mathbf{k}} + \gamma_{\mathbf{k}} \cos 2\varphi_{1,2})(J_0 + J_{\mathbf{k}})$$

$$\epsilon_{\mathbf{k}\,out}^2 = S^2(J_0 - J_{\mathbf{k}} + I_0 - I_{\mathbf{k}} + A_{\mathbf{k}})(J_0 + J_{\mathbf{k}}), \tag{34}$$

where we neglected $I_0, A_{\mathbf{k}}$ and P comparing to $J_0 + J_{\mathbf{k}}$ and $\mathbf{k}$ belongs to the magnetic zone. These expressions coincide with those given in Refs. 21 and 22, if according to Ref. 23 we set $J = J_{av}$, $A = J_{av} - J_z$, $P = \delta J$ and neglect $I_{\mathbf{k}}$. We see that the in-plane branch remains gapless despite the fact that the PD interaction violates the rotational invariance around the c axis. As we will show below a corresponding gap appears as a result of the interaction between spin waves. The out-of-plane gap has the form

$$\Delta_{out}^2 = 8S^2 J_0 A = 32 S^2 J A. \tag{35}$$

Let us consider now the interaction between adjacent planes. It is very small and has to be taken into account only along the directions $(0,0,k_c)$ and (k_{0a}, k_{0b}, k_c). Otherwise it is masked by the dispersion connected with the huge intraplane exchange. As a result the in-plane mode splits to acoustic and optical branches and using Eqs. (18), (19), (23)–(25), and (32) we obtain

$$\epsilon_{ac}^2(k_c) = 2SJ_0\left\{2SI(1-\cos k_c) + R_0\left[1 - \cos\frac{k_c}{2}\right]\right\}$$

$$\epsilon_{opt}^2(k_c) = 2SJ_0\left\{2SI(1-\cos k_c) + R_0\left[1 + \cos\frac{k_c}{2}\right]\right\}. \tag{36}$$

In the considered approximation the out-of-plane mode remains unsplit and instead of Eq. (35) we get

$$\Delta_{out}^2 = 2SJ_0(4SA + R_0). \tag{37}$$

Thus, we see that the interplane PD interaction gives a contribution to the out-of-plane spin-wave gap too.

IV. INTRAPLANE ANISOTROPY

In this section, we obtain the φ-dependent contribution to the ground-state energy that gives rise to the square anisotropy considered in Refs. 21 and 22. This anisotropy is responsible for the spin-wave gap in the in-plane mode. In Refs. 21 and 22 this gap has been calculated using an effective Hamiltonian. We demonstrate that it appears as a result of interaction between spin waves and determine the φ dependence of the gap, which is important in the case of nonzero magnetic field (see Sec. VII). We show also that this interaction leads to replacement in Eq. (35) the spin value S by $\langle S_z \rangle$ as has been assumed in Ref. 22.

According to Refs. 21 and 22 the first correction to the ground-state energy is given by zero-point motion and has the form

$$\Delta E = \tfrac{1}{2}\sum_{\mathbf{k}} (\epsilon_{\mathbf{k}} - E_{\mathbf{k}}), \tag{38}$$

where the sum is extended over the whole Brillouin zone; $\epsilon_{\mathbf{k}}$ and $E_{\mathbf{k}}$ are given by Eqs. (23) and (33). Neglecting all small interactions (except for the intraplane PD for a single plane) we get the φ-dependent part of this energy in the following form:

$$\Delta E_{\varphi} = \frac{N\Delta_0^2}{16 J_0} \sin^2 2\varphi, \tag{39}$$

where we replaced $\varphi_{1,2}$ on φ and

$$\Delta_0^2 = \frac{2SP^2}{(2\pi)^2}\int_{-\pi}^{\pi} dk_a dk_b \frac{(2 + \cos k_a + \cos k_b)^{1/2}}{(2 - \cos k_a - \cos k_b)^{3/2}} \times (\cos k_a - \cos k_b)^2 \simeq 1.28 SP^2. \tag{40}$$

These expressions coincide with the results of Refs. 21 and 22.

Using Eqs. (20) and (39) for the energy that determines the ground-state configuration of the system we get

$$E_0 = S^2 N J_0 \left[\frac{\Delta_0^2}{4(2SJ_0)^2} (\sin^2 2\varphi_1 + \sin^2 2\varphi_2) + \frac{8Q_0}{J_0} \sin(\varphi_1 + \varphi_2) \right]. \quad (41)$$

Here the first two terms are minimal at $\varphi_{1,2} = 0, \pi/2$ and determine $\hat{a}$ and $\hat{b}$ as easy axes. The second term has a minimum at $\varphi_1 + \varphi_2 = -\pi/2$ for positive Q_0 and $\varphi_1 + \varphi_2 = \pi/2$ for $Q_0 < 0$. As a result the whole expression (41) determines the first (La_2NiO_4) and the second (La_2CuO_4) types of the structure shown in Fig. 1(b) for $Q > 0$ and $Q < 0$, respectively.

From Eq. (39), one sees that the PD interaction gives rise to square anisotropy, which should be responsible for the gap in the in-plane spin-wave mode. In Ref. 22 this gap has been determined using a specially constructed effective Hamiltonian. We will demonstrate now that the lowest order perturbation theory gives the same result. We will determine also the φ dependence of the gap, which is essential for description of the system in magnetic field (see Sec. VII).

Using Eqs. (10)–(16), we represent the interaction energy in the following form:

$$V = V_3 + V_4 + V_5 + V_6, \quad (42)$$

where V_n is responsible for the interaction between n spin waves. We restrict ourselves to the one-plane problem. In this case we have

$$V_3 = i \left(\frac{S}{2N} \right)^{1/2} \sin 2\varphi \sum \gamma_{\mathbf{k}_1} a^+_{\mathbf{k}_1 + \mathbf{k}_2} a_{\mathbf{k}_2} (a_{\mathbf{k}_1} - a^+_{-\mathbf{k}_1}). \quad (43)$$

The fourth-order interaction is a sum $V_4 = V_4^{(1)} + V_4^{(2)} + V_4^{(3)}$, where

$$V_4^{(1)} = -\frac{1}{2N} \sum V^{(1)}_{\mathbf{k}_3} a^+_{\mathbf{k}_3 + \mathbf{k}_1} a^+_{-\mathbf{k}_3 + \mathbf{k}_2} a_{\mathbf{k}_1} a_{\mathbf{k}_2},$$

$$V_4^{(2)} = -\frac{1}{2N} \sum V^{(2)}_{\mathbf{k}_3} a^+_{\mathbf{k}_3 + \mathbf{k}_1 + \mathbf{k}_2} a_{\mathbf{k}_1} a_{\mathbf{k}_2} a_{\mathbf{k}_3}, \quad (44)$$

$$V_4^{(3)} = -\frac{1}{2N} \sum V^{(3)}_{\mathbf{k}_3} a^+_{\mathbf{k}_3} a^+_{-\mathbf{k}_3 + \mathbf{k}_1 + \mathbf{k}_2} a_{\mathbf{k}_1} a_{\mathbf{k}_2}.$$

Here

$$V^{(1)}_{\mathbf{k}} = J_{\mathbf{k}} + \gamma_{\mathbf{k}} \cos 2\varphi,$$

$$V^{(2)}_{\mathbf{k}} = J_{\mathbf{k}} - \tfrac{1}{2} A_{\mathbf{k}} - \tfrac{1}{2} \gamma_{\mathbf{k}} \cos 2\varphi, \quad (45)$$

$$V^{(3)}_{\mathbf{k}} = -\tfrac{1}{2} A_{\mathbf{k}} + \tfrac{1}{2} \gamma_{\mathbf{k}} \cos 2\varphi,$$

and $\gamma_{\mathbf{k}}$ is determined by Eq. (24). The interactions V_5 and V_6 will not be used below and we do not give here corresponding expressions.

Now, it is worth pointing out the non-Hermiticy of the interactions $V_4^{(2,3)}$, which is a direct consequence of the representation (12) for the spin operators. As a result in the intermediate steps of the calculations some quantities do not exhibit the conventional properties. For example, the equality $F^+_{\mathbf{k}}(\omega) = F_{\mathbf{k}}(-\omega)$ is broken, where F^+ and F are the Green's functions determined by Eq. (28). The consequence of the Hermiticity of the initial physical problem is restored in the final results only. For example the spin Green's function contains the sum $F^+ + F$. The similar situation takes place in the spin techniques by Vaks, Larkin, and Pikin[29] too. It may be shown that for $T \ll T_N$ both techniques are equivalent.

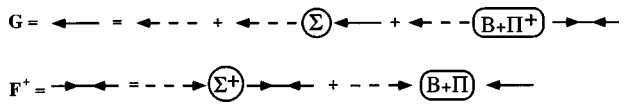

FIG. 4. Belyaev's equations for the Green's functions G and F^+. The left and right broken arrows represent the bare Green's functions $G_{0\mathbf{k}}(\omega)$ and $G^+_{0\mathbf{k}}(\omega) = G_{0\mathbf{k}}(-\omega)$, respectively, where $G_{0\mathbf{k}}(\omega) = (\omega - E_{\mathbf{k}})^{-1}$. The values $E_{\mathbf{k}}$ and $B_{\mathbf{k}}$ are given by Eq. (23).

Below we will use the conventional diagrammatic techniques[30] for calculations of the Green's functions and we take into account diagrams containing one sum over intermediate momenta. This approximation gives the first term of $1/S$ expansion and has been used in Refs. 31 and 32 for determination corrections to the spin-wave spectrum in the exchange approximation. The real justification of this approximation is some small numerical coefficients that should appear at each additional momentum summation. Obviously, the interactions V_5 and V_6 should be omitted in this approximation.

Above we did not diagonalize the Hamiltonian (22) and had two kinds of Green's functions G, G^+, F, and F^+ determined by Eq. (28). As a result diagrammatic techniques used below should be similar to the Beliaev one,[30,33] which has been developed for the diluted Bose-Gas below T_c. The only distinction is related to the non-Hermiticity of the interaction due to which we have $G^+(\omega) \neq G(-\omega)$ and $F^+(\omega) \neq F(\omega)$. In this case we have a system of Dyson equations determining self-energy parts Σ, Σ^+, Π, and Π^+. Equations for G and F^+ are shown in Fig. 4. Other two equations for G^+ and F have similar structure. Solution of these equations is given by

$$G = (\omega + \xi_{\mathbf{k}}) D^{-1}, \quad G^+ = (-\omega + \xi^+_{\mathbf{k}}) D^{-1}$$
$$F^+ = -\beta_{\mathbf{k}} D^{-1}, \quad F = -\beta^+_{\mathbf{k}} D^{-1}, \quad (46)$$

where

$$\xi_{\mathbf{k}} = E_{\mathbf{k}} + \Sigma_{\mathbf{k}}, \quad \xi^+_{\mathbf{k}} = E_{\mathbf{k}} + \Sigma^+_{\mathbf{k}},$$
$$\beta_{\mathbf{k}} = B_{\mathbf{k}} + \Pi_{\mathbf{k}}, \quad \beta^+_{\mathbf{k}} = B_{\mathbf{k}} + \Pi^+_k, \quad (47)$$
$$D = \omega^2 - (\xi_{\mathbf{k}} \xi^+_{\mathbf{k}} - \beta_{\mathbf{k}} \beta^+_{\mathbf{k}}).$$

Here $E_{\mathbf{k}}$ and $B_{\mathbf{k}}$ are given by Eqs. (23). Neglecting Σ, Π, and Π^+ we have

$$G = (\omega + E_{\mathbf{k}})(\omega^2 - \epsilon^2_{\mathbf{k}})^{-1},$$
$$F = F^+ = -B_{\mathbf{k}} (\omega^2 - \epsilon^2_{\mathbf{k}})^{-1}. \quad (48)$$

These equations actually follow from Eq. (30) if one neglects the interaction between subsystems.

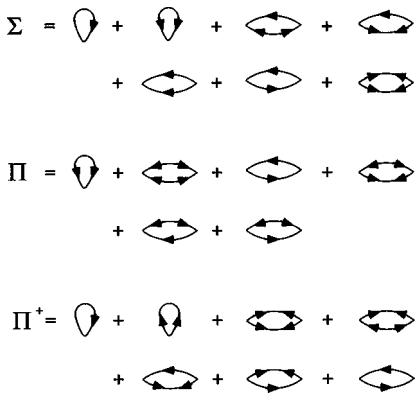

FIG. 5. The first-order diagrams for the self-energies Σ, Π, and Π^+, which contribute at $\mathbf{k}=(0,0,q_c)$ and $\mathbf{k}=(\mathbf{k_0},q_c)$. The self-energy Σ^+ is determined by the same set of diagrams as Σ with inversion of the directions of all arrows.

From Eqs. (47) for the spin-wave energy in the first approximation described above we have

$$\epsilon_{\mathbf{k}R}^2=\epsilon_{\mathbf{k}}^2+\delta\epsilon_{\mathbf{k}}^2,$$
$$\delta\epsilon_{\mathbf{k}}^2=E_{\mathbf{k}}(\Sigma_{\mathbf{k}}+\Sigma_{\mathbf{k}}^+)-B_{\mathbf{k}}(\Pi_{\mathbf{k}}+\Pi_{\mathbf{k}}^+). \tag{49}$$

Corresponding diagrams for $\Sigma_{\mathbf{k}}=(\Sigma_{\mathbf{k}}^+)^*$, $\Pi_{\mathbf{k}}$, and $\Pi_{\mathbf{k}}^+$ are shown in Fig. 5. They are divided on the one-vertex Hartree-Fock and two-vertex propagative diagrams related to interactions V_4 and V_3, respectively.

Analytical expressions for the Hartree-Fock diagrams are given by

$$\Sigma_{\mathbf{k}}=\Sigma_{\mathbf{k}}^+=-\frac{1}{N}\sum_{\mathbf{k_1}}\left\{[V_0^{(1)}+V_{\mathbf{k}-\mathbf{k_1}}^{(1)}+V_{\mathbf{k}}^{(3)}+V_{\mathbf{k_1}}^{(3)}]n_{\mathbf{k_1}}+\left[\frac{1}{2}V_{\mathbf{k}}^{(2)}+V_{\mathbf{k_1}}^{(2)}\right]f_{\mathbf{k_1}}\right\}, \tag{50}$$

$$\Pi_{\mathbf{k}}=-\frac{1}{N}\sum_{\mathbf{k_1}}[V_{\mathbf{k}-\mathbf{k_1}}^{(1)}+V_{\mathbf{k}-\mathbf{k_1}}^{(3)}]f_{\mathbf{k_1}},$$

$$\Pi_{\mathbf{k}}^+=-\frac{1}{N}\sum_{\mathbf{k_1}}\{[V_{\mathbf{k_1}}^{(2)}+2V_{\mathbf{k}}^{(2)}]n_{\mathbf{k_1}}+[V_{\mathbf{k}-\mathbf{k_1}}^{(1)}+V_{\mathbf{k_1}}^{(3)}]f_{\mathbf{k_1}}\}, \tag{51}$$

where $V_{\mathbf{k}}^{(i)}$ are determined by Eqs. (45) and

$$n_{\mathbf{k}}=\langle a_{\mathbf{k}}^+ a_{\mathbf{k}}\rangle=\frac{E_{\mathbf{k}}-\epsilon_{\mathbf{k}}}{2\epsilon_{\mathbf{k}}},$$
$$f_{\mathbf{k}}=\langle a_{\mathbf{k}}^+ a_{-\mathbf{k}}^+\rangle=\langle a_{\mathbf{k}}a_{-\mathbf{k}}\rangle=-\frac{B_{\mathbf{k}}}{2\epsilon_{\mathbf{k}}}. \tag{52}$$

If we neglect the anisotropy and the PD interaction, Eqs. (49), (50), and (51) give the well-known expression to the first-order renormalization of the spin-wave energy:[31,32]

$$\epsilon_{\mathbf{k}R}^2=\epsilon_{\mathbf{k}}^2\left\{1+\frac{1}{S}-\frac{1}{2SN}\sum_{\mathbf{k}}[4-(\cos k_a+\cos_b)^2]^{1/2}\right\}\simeq\epsilon_{\mathbf{k}}^2(1-0.16/S). \tag{53}$$

Equations (49) and (50) at $\mathbf{k}=\mathbf{k}_0$ give renormalization of the out-of-plane gap assumed in Ref. 22 and instead of Eq. (35) we have

$$\Delta_{out}^2=8\langle S\rangle^2 J_0 A, \tag{54}$$

where $\langle S\rangle$ is the average z component of the spin, reduced by the zero-point fluctuations

$$\langle S\rangle=S\left[1-\frac{1}{NS}\sum_{\mathbf{k}}n_{\mathbf{k}}\right]\simeq S\left(1-\frac{0.20}{S}\right). \tag{55}$$

At $\mathbf{k}=0$ the Hartree-Fock contribution to the in-plane gap is given by

$$\Delta_{HF}^2=\Delta_{01}^2=\Delta_0^2\cos^2 2\varphi, \tag{56}$$

where Δ_0^2 is determined by Eq. (40).

The two-vertex diagrams shown in Fig. 5 at $\mathbf{k}=0$ and $\omega=0$ give the expressions

$$\Sigma_0=(\Sigma_0^+)^*=\frac{S}{2N}T\sum_{\mathbf{k},\omega}\gamma_{\mathbf{k}}^2[4F_{\mathbf{k}}(i\omega)G_{\mathbf{k}}(i\omega)-2G_{\mathbf{k}}^2(i\omega)-F_{\mathbf{k}}^2(i\omega)-G_{\mathbf{k}}(i\omega)G_{\mathbf{k}}(-i\omega)]\sin^2 2\varphi, \tag{57}$$

$$\Pi_0=\Pi_0^+=\frac{S}{2N}T\sum_{\mathbf{k},\omega}\gamma_{\mathbf{k}}^2\{3F_{\mathbf{k}}^2(i\omega)+G_{\mathbf{k}}(i\omega)G_{-\mathbf{k}}(-i\omega)-2F_{\mathbf{k}}(i\omega)[G_{\mathbf{k}}(i\omega)+G_{\mathbf{k}}(-i\omega)]\}\sin^2 2\varphi,$$

where ω is Matsubara frequency. After simple calculations, we obtain the following contribution to the in-plane gap:

$$\Delta_{02}^2=-\Delta_0^2\sin^2 2\varphi. \tag{58}$$

As a result we have the final expression for the in-plane gap:

$$\delta\epsilon_0^2=\Delta_{in}^2=\Delta_0^2\cos 4\varphi, \tag{59}$$

where Δ_0^2 is given by Eq. (40). For $\varphi=0$ this expression coincides with the result of Ref. 22. However as we will see in Sec.VII the φ dependence of the in-plane gap becomes important in magnetic field. Proportional to P^2 correction to Δ_{out}^2 appears too [see Eq. (109) in Sec. IX)]. However as we will see below $\Delta_{out}^2\gg\Delta_{in}^2$ and it may be neglected. For the ground-state configuration we have $\varphi_1=0$ and $\varphi_2=\pm\pi/2$. In this case instead of Eqs. (36) for acoustic and optical spin-wave branches along $(0,0,k_c)$ direction we get

$$\epsilon_{ac}^2=2SJ_0\left[2SI(1-\cos k_c)+R_0\left(1-\cos\frac{k_c}{2}\right)\right]+\Delta_0^2,$$
$$\epsilon_{opt}^2=2SJ_0\left[2SI(1-\cos k_c)+R_0\left(1+\cos\frac{k_c}{2}\right)\right]+\Delta_0^2, \tag{60}$$

where R_0 is given by Eq. (24). Summarizing results given by Eqs. (37) and (54) for the out-of-plane mode along the same direction we obtain

$$\Delta_{out}^2=8\langle S\rangle^2 J_0 A+2SJ_0R_0, \tag{61}$$

where $\langle S\rangle$ is determined by Eq. (55).

It should be emphasized that the φ dependence of the in-plane gap given by Eq. (59) is not a specific result of the PD interaction (7). In fact it is a direct consequence of the square symmetry of CuO_2 planes. Indeed, in a general form the square anisotropy is given by

$$H_{sq}=\sum_{\mathbf{k}_1+\mathbf{k}_2+\mathbf{k}_3+\mathbf{k}_4=0}\times[\lambda_1(S_1^aS_2^aS_3^aS_4^a+S_1^bS_2^bS_3^bS_4^b)+\lambda_2S_1^aS_2^aS_3^bS_4^b], \tag{62}$$

where $\mathbf{S}_i=\mathbf{S}_{\mathbf{k}_i}$. This expression may be represented in the following form:

$$H_{sq}=\sum_{\mathbf{k}_1+\mathbf{k}_2+\mathbf{k}_3+\mathbf{k}_4=0}[\lambda_1(S_1^aS_2^a+S_1^bS_2^b)\times(S_3^aS_4^a+S_3^bS_4^b)+\lambda S_1^aS_2^aS_3^bS_4^b], \tag{63}$$

where $\lambda=\lambda_2-2\lambda_1$. Here the first term is invariant under rotation in the (a,b) plane and then contributes to the uniaxial anisotropy only. From the second term using Eq. (11) and linear spin-wave theory we get

$$H_{sq}=\frac{\lambda NS^4}{4}\sin^2 2\varphi+\lambda S^3\times\sum_{\mathbf{k}}[(\cos^4\varphi+\sin^4\varphi-8\sin^2\varphi\cos^2\varphi)a_{\mathbf{k}}^+a_{\mathbf{k}}+\tfrac{1}{2}(a_{\mathbf{k}}a_{-\mathbf{k}}+a_{-\mathbf{k}}^+a_{\mathbf{k}}^+)(4\sin^2\varphi\cos^2\varphi-\cos^4\varphi-\sin^4\varphi)]. \tag{64}$$

Here the first term should be added to the ground-state energy (41) and the second one contributes to $E_{\mathbf{k}}$ and $B_{\mathbf{k}}$ in Eq. (22). As a result the spin-wave gaps given by Eqs. (59) and (61) acquire the following additional terms:

$$\delta\Delta_{in}^2=4S^4J_0\lambda\cos 4\varphi, \tag{65}$$

$$\delta\Delta_{out}^2=-2S^4J_0\lambda\sin^2 2\varphi. \tag{66}$$

We see that $\delta\Delta_{in}^2$ is proportional to $\cos 4\varphi$ as in expression (59). If Eq. (64) gives only the contribution to the anisotropy we have the $\hat{a}$ and $\hat{b}$ as easy directions ($\varphi=0,\pm\pi/2$) for positive λ and $\delta\Delta_{out}^2=0$. For $\lambda<0$ the direction [1,1,0] is the easy axis ($\varphi=\pm\pi/4$) and both expressions (65) and (66) are positive.

As we will see in the end of Sec. IX the value of the in-plane gap depends strongly on the environment of the CuO_2 planes and particularly on the type of rare-earth ion. This dependence may be attributed to the PD interaction as well as to an additional square anisotropy.

V. NONCOLLINEARITY AND NEUTRON SCATTERING

In this section, we present expressions for the elastic and inelastic neutron scattering cross sections, which have some peculiarities connected with the noncollinear magnetic structure of the R_2CuO_4 family. Corresponding experimental results will be considered in the next section.

We begin with the elastic scattering cross section, normalized on the chemical unit cell, which has the following form:

$$\frac{d\sigma}{d\Omega}=[r_0\langle S\rangle F(\mathbf{Q})]^2\left\{2-\frac{(\mathbf{Q}\cdot\hat{e}_{z_1})^2}{Q^2}-\frac{(\mathbf{Q}\cdot\hat{e}_{z_2})^2}{Q^2}+2\left[(\hat{e}_{z_1}\cdot\hat{e}_{z_2})-\frac{(\mathbf{Q}\cdot\hat{e}_{z_1})(\mathbf{Q}\cdot\hat{e}_{z_2})}{Q^2}\right]\times\cos(\mathbf{Q}\cdot\boldsymbol{\delta})\right\}\frac{(2\pi)^3}{V_0}\delta(\mathbf{Q}+\boldsymbol{\tau}_{AF}), \tag{67}$$

where $r_0^2=0.292$ barns for magnetic scattering, $F(\mathbf{Q})$ is the magnetic form factor of Cu^{2+} ions, $\langle S\rangle$ is their average spin, $\hat{e}_{z_{1,2}}$ are directions of the subsystem magnetization given by Eq. (11), and V_0 is the unit-cell volume, $\boldsymbol{\tau}_{AF}=\boldsymbol{\tau}+k_0$ where $\boldsymbol{\tau}$ and $\mathbf{k_0}$ are reciprocal vectors of the chemical and magnetic lattices respectively.

The magnetic structure factor is determined by angles φ_1 and φ_2, which depend on the magnetic field $\mathbf{H}$ (see Sec. VII). If $H=0$, we have $\varphi_1=0$ and $\varphi_2=(-1)^t\pi/2$ where $t=1$ and $t=2$ for the first and the second type of the structure shown in Fig. 1(b), respectively.

In this case, for the reflections $\mathbf{Q}=(k/2,\pm k/2,\ell)$, where k is an odd number, the expression inside brackets in Eq. (67) is given by

$$\begin{aligned}&2, \quad \ell+t \text{ is even;}\\ &2\frac{Q_c^2}{Q^2}=\frac{2(a/c)^2\ell^2}{k^2/2+(a/c)^2\ell^2}, \quad \ell+t \text{ is odd.}\end{aligned} \tag{68}$$

In particular, if $\ell=0$, the elastic scattering is forbidden for the first type of the structure with $t=1$.

The angles φ_1 and φ_2 are complicated functions of the field. However, if $\mathbf{H}$ is along the [110] direction according to the results of Sec. VII, we have $\varphi_2=(-1)^t\pi/2-\varphi_1$, $0>\varphi_1>-\pi/4$ if $g\mu H<g\mu H_c=\Delta_0$ and $\varphi_1=-\pi/4$ if $H\geqslant H_c$.

In this case for the reflections $Q=(k/2,-k/2,\ell)$ instead of Eq. (68) we get

$$\begin{aligned}&2(1+\sin 2\varphi_1), \quad \ell+t \text{ is even;}\\ &2(1-\sin 2\varphi_1)\frac{Q_c^2}{Q^2}=\frac{2(a/c)^2\ell^2}{k^2/2+(a/c)^2\ell^2}(1-\sin 2\varphi_1),\\ &\ell+t \text{ is odd.}\end{aligned} \tag{69}$$

The consequences of these expressions have been used in Refs. 1–5 for establishing the spin structure [La_2CuO_4/La_2NiO_4 type, see Fig. 1(b)] observed in the different members of the R_2CuO_4 family. In addition, Eq. (69) has allowed one to establish the noncollinearity by applying a field slightly off from the $\hat{a}$ direction.[3,4]

We now consider the inelastic neutron scattering. It was studied in R_2CuO_4 systems in zero magnetic field only and

here we mainly restrict ourselves to this case. Results for $H \neq 0$ are considered briefly in Sec. VIII. The main problem is the consideration of the interference between adjacent planes with noncollinear magnetic ordering. This interference is important for the in-plane spin-wave scattering and along the directions $\mathbf{Q}=(h/2,k/2,q_c)$ only where h and k are odd integer numbers and contribution to the spin-wave energy of the very strong intraplane exchange interaction disappears. Corresponding experimental results are presented in the next section.

In inelastic neutron scattering, the measured cross sections can be always written in terms of the scattering function, $S(\mathbf{Q},\omega)$, as

$$\left(\frac{d^2\sigma}{d\Omega\, d\omega}\right)=r_0^2F(\mathbf{Q})^2\frac{k_F}{k_I}S(\mathbf{Q},\omega) \tag{70}$$

with the notations of Eq. (67) and where k_F/k_I is the usual kinematic ratio of final neutron wave vector k_F to the incident one k_I. We begin with the general expressions for the spin-wave scattering function. For the out-of-plane spin waves, it has the form

$$\begin{aligned}S_{out}(\mathbf{Q},\omega)=&\left(1-\frac{Q_c^2}{Q^2}\right)\{S_{c_1,c_1}(\mathbf{q},\omega)+S_{c_2,c_2}(\mathbf{q},\omega)\\&+[S_{c_1,c_2}(\mathbf{q},\omega)+S_{c_2,c_1}(\mathbf{q},\omega)]\cos(\mathbf{Q}\cdot\boldsymbol{\delta})\},\end{aligned} \tag{71}$$

where $\mathbf{Q}=\boldsymbol{\tau}+\mathbf{q}$, $\boldsymbol{\tau}$ is the reciprocal lattice vector and $Q_c=(2\pi/c)q_c$.

For the in-plane spin waves, the scattering function may be represented as

$$\begin{aligned}S_{in}(\mathbf{Q},\omega)=&\left\{S_{y_1,y_1}(\mathbf{q},\omega)\left(1-\frac{Q_{y_1}^2}{Q^2}\right)\right.\\&+S_{y_2,y_2}(\mathbf{q},\omega)\left(1-\frac{Q_{y_2}^2}{Q^2}\right)\\&+[S_{y_1,y_2}(\mathbf{q},\omega)+S_{y_2,y_1}(\mathbf{q},\omega)]\\&\left.\times\left(\hat{e}_{y_1}\hat{e}_{y_2}-\frac{Q_{y_1}Q_{y_2}}{Q^2}\right)\cos[(\mathbf{Q}-\mathbf{k}_0)\cdot\boldsymbol{\delta}]\right\},\end{aligned} \tag{72}$$

where $y_{1,2}$ are y axes for subsystems 1 and 2, $\hat{e}_{y1}$ and $\hat{e}_{y2}$ are corresponding units vectors given by Eq. (11), and $\mathbf{Q}=\boldsymbol{\tau}+q+k_0$. According to our choice $\mathbf{k}_0=\mathbf{k}_0^{(2)}$ [see Eq. (10)], and $\boldsymbol{k}_0\cdot\boldsymbol{\delta}=0$. However, it is convenient to retain this term in Eq. (72).

In Eqs. (71) and (72), the partial scattering functions are determined by application of the fluctuation-dissipation theorem,

$$S_{\lambda',\lambda}(\mathbf{q},\omega)=\frac{1}{\pi}\frac{1}{1-\exp(-\omega/k_BT)}\mathrm{Im}\,\chi_{\lambda',\lambda}(\mathbf{q},\omega), \tag{73}$$

where $\chi_{\lambda'\lambda}$ is the associated susceptibility, which is determined by Eq. (26) with change of sign and if A and B are the spin operators, $S_{\lambda'}$ and S_{λ}, respectively. Using this definition we get from Eqs. (12) and (28)

$$\begin{aligned}\chi_{c_{\lambda'},c_{\lambda}}(\omega)=&-\frac{S}{2}[G_{\lambda',\lambda}(\omega)+G_{\lambda',\lambda}(-\omega)\\&+F_{\lambda',\lambda}(\omega)+F^{+}_{\lambda',\lambda}(\omega)]\\\chi_{y_{\lambda'},y_{\lambda}}(\omega)=&-\frac{S}{2}[G_{\lambda',\lambda}(\omega)+G_{\lambda',\lambda}(-\omega)\\&-F_{\lambda',\lambda}(\omega)-F^{+}_{\lambda',\lambda}(\omega)].\end{aligned} \tag{74}$$

The functions G,F,F^+ in a magnetic field are given by Eqs. (B13) and (B20). However, for $H=0$, we can use Eq. (30) replacing Δ by

$$\Delta_1(\omega)=(\omega^2-\epsilon_{ac}^2)(\omega^2-\epsilon_{opt}^2), \tag{75}$$

where ϵ_{ac}^2 and ϵ_{opt}^2 are given by Eqs. (60) if $q_a=q_b=0$, and $\Delta_1(\omega)=(\omega^2-\Delta_{out}^2)^2$ for $q_a=\pm q_b=1/2$. As a result, we have

$$\begin{aligned}\chi_{c_1,c_1}=\chi_{c_2,c_2}=&-S^2(J_0-J_{\mathbf{q}})(\omega^2-\epsilon^2)/(2\Delta_1),\\\chi_{c_1,c_2}=\chi_{c_2,c_1}=&-S^2(J_0-J_{\mathbf{q}})(C+D)/(2\Delta_1),\\\chi_{y_1,y_1}=\chi_{y_2,y_2}=&-S^2(J_0+J_{\mathbf{q}})(\omega^2-\epsilon^2)/(2\Delta_1),\\\chi_{y_1,y_2}=\chi_{y_2,y_1}=&-S^2(J_0+J_{\mathbf{q}})(C-D)/(2\Delta_1),\end{aligned} \tag{76}$$

where $\epsilon^2=(\epsilon_{ac}^2+\epsilon_{opt}^2)/2$, C and D are given by Eq. (25).

For the out-of-plane spin wave $\mathbf{Q}=\boldsymbol{\tau}+\mathbf{q}$ and if $q_a=q_b=0$, we have $\chi_{c_{\lambda'},c_{\lambda}}=0$ and the neutron scattering is forbidden. It becomes maximal for $q_a=\pm q_b=1/2$, i.e., at the AF Bragg rods. However, along these lines we have $C+D=0$ and the interference disappears. As a result for $\mathbf{Q}\simeq\boldsymbol{\tau}_{AF}$ and $\omega>0$ we obtain

$$S_{out}(\mathbf{Q},\omega)=\left(1-\frac{Q_c^2}{Q^2}\right)\frac{1}{\Delta_{out}}\frac{S^2J_0\delta(\omega-\Delta_{out})}{1-\exp(-\omega/k_BT)}. \tag{77}$$

For the in-plane spin waves, $\mathbf{Q}=\boldsymbol{\tau}_{AF}+\mathbf{q}$ and along the magnetic lines, we have $\mathbf{q}=(0,0,q_c)$. Taking into account that $\epsilon_{opt}^2-\epsilon_{ac}^2=4SJ_0(C-D)$ [see Eqs. (25) and (60)], the cross section for $\omega>0$ may be represented as follows:

$$\begin{aligned}S_{in}(\mathbf{Q},\omega)=&\frac{S^2J_0}{2[1-\exp(-\omega/k_BT)]}\\&\times\left\{\left[1+\frac{Q_c^2}{Q^2}-2\frac{Q_{y_1}Q_{y_2}}{Q^2}\cos(\boldsymbol{\tau}_{AF}\cdot\boldsymbol{\delta})\right]\frac{\delta(\omega-\epsilon_{opt})}{\epsilon_{opt}}\right.\\&\left.+\left[1+\frac{Q_c^2}{Q^2}+2\frac{Q_{y_1}Q_{y_2}}{Q^2}\cos(\boldsymbol{\tau}_{AF}\cdot\boldsymbol{\delta})\right]\frac{\delta(\omega-\epsilon_{ac})}{\epsilon_{ac}}\right\}.\end{aligned} \tag{78}$$

This expression is written for all values of q_c. We below refer to the branches that have a minus and a plus sign in Eqs. (60) as acoustic and optical excitations, respectively. For the first (La_2NiO_4) and the second (La_2CuO_4) type systems shown in Fig. 1(b), we have $\varphi_2=-\pi/2$, $\hat{e}_{y_2}=\hat{a}$ and $\varphi_2=\pi/2$, $\hat{e}_{y_2}=-\hat{a}$, respectively. As a result, the interference terms in Eq. (78) have different sign in these two cases and this equation may be rewritten as

$$S_{in}(\mathbf{Q},\omega)=\frac{S^2J_0}{2[1-\exp(-\omega/k_BT)]}\times\left\{\left[1+\frac{Q_c^2}{Q^2}+2(-1)^t\frac{Q_aQ_b}{Q^2}\cos(\boldsymbol{\tau}_{AF}\cdot\boldsymbol{\delta})\right]\times\frac{\delta(\omega-\epsilon_{opt})}{\epsilon_{opt}}+\left[1+\frac{Q_c^2}{Q^2}-2(-1)^t\frac{Q_aQ_b}{Q^2}\times\cos(\boldsymbol{\tau}_{AF}\cdot\boldsymbol{\delta})\right]\frac{\delta(\omega-\epsilon_{ac})}{\epsilon_{ac}}\right\}, \quad (79)$$

where $t=1$ stands for the La_2NiO_4 case and $t=2$ for the La_2CuO_4 case.

The interference becomes very important at $\mathbf{Q}=(1/2,1/2,0)$. In this case $\cos(\boldsymbol{\tau}_{AF}\cdot\boldsymbol{\delta})=-1$, and acoustic and optical branches do not contribute to the neutron cross section for $t=1$ and $t=2$, respectively. The disappearance of the scattering on the acoustic branch observed in Pr_2CuO_4 ($t=1$) and discussed in the next section.

VI. EXPERIMENTAL RESULTS

In this section, we present results of the inelastic neutron scattering experiments in Pr_2CuO_4. We deduce from them the main theoretical parameters: the strength of the intraplane (P) and interplane (Q) pseudodipolar interactions. Available experimental results for the inelastic neutron scattering in Nd_2CuO_4 (Ref. 14) will be discussed too.

A. Experimental procedure

The Pr_2CuO_4 single crystal of very good mosaicity (less than 10′) and with $T_N=247$ K was grown in air from the melt in a crucible. The sample, already used in higher-energy spin-wave experiments[35] as well as in Ref. 18, was a plate of about a volume of 0.5 cm^3. It was mounted with the reciprocal directions (110) and (001) within the scattering plane. Inelastic neutron scattering experiments were performed using the triple-axis spectrometers at the thermal neutron beam 2 T and at the cold neutron beam 4F1 of Laboratoire Léon Brillouin at the reactor Orphée (Saclay). Monochromator and analyzer were of pyrolytic graphite. The analyzer was focussed horizontally on 4F1 and horizontally and vertically on 2 T to improve the intensity using no collimation. On thermal beam, we worked in constant-k_F mode with $k_F=2.662$ Å^{-1} leading to typical energy resolution of 1 meV. A graphite filter was put in the scattered beam to remove neutrons with wave vectors $2k_F$. Cold neutron experiments were performed on spectrometer 4F1 in the range 0.1–4.0 meV. We used both constant-k_F and constant-k_I modes with $k_{I,F}=1.55$ Å^{-1} for the higher-energy part and constant-k_F mode at $k_F=1.15$ Å^{-1} for the lowest energies investigated. This gives a typical energy resolution at $\hbar\omega=0$ (full width at half-maximum) of 0.2 and 0.1 meV, respectively. Multiple-order contamination in the scattered beam was removed by a beryllium filter and the results are corrected for efficiency and influence of multiple order on the monitor as a function of k_I.

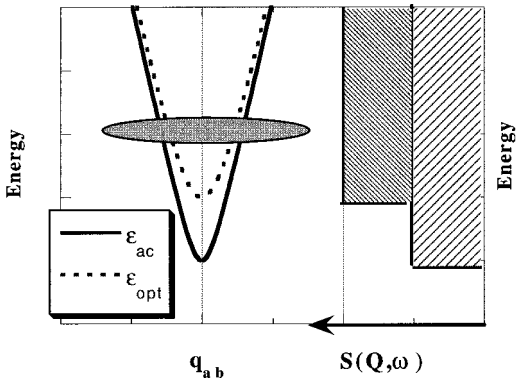

FIG. 6. Left part: In-plane spin-wave dispersion curves for AF undoped cuprates R_2CuO_4 along the magnetic rod. The ellipse sketches the experimental resolution function. Right part: schematic representation of the energy dependence of the measured integrated intensity, see text for details. The temperature factor is not included.

B. In-plane q integration due to the ellipsoid resolution

The strong in-plane superexchange coupling in cuprates ($J>100$ meV), implying very large in-plane spin-wave velocity c_0 put severe constraints on the neutron scattering methods. A typical in-plane dispersion curve is schematically drawn in Fig. 6. The key point is that the in-plane q resolution (the size of the ellipse in Fig. 6), is always larger than the in-plane wave vector of the spin waves $q_{SW}=\omega/c_0$. That is the case for the whole energy range (0.1–12 meV) investigated here. The separation of the counterpropagating spin waves (from q and $-q$) in the (q_a,q_b) plane may be done in the high-energy region[1] or using an adapted focalized geometry.[35] Accordingly, in our case spin-wave branches do not show up as two individual peaks in an in-plane q scan at constant energy. The measured intensity for such q scans is rather a single peak of roughly the q width of the resolution centered on the magnetic rod (see Fig. 9). Such sharp peaks around the AF wave vector sign the magnetic origin of the scattering. A further consequence is that the scattered intensity measured at the antiferromagnetic line, $\mathbf{Q}=(1/2,1/2,q_c)$, is not simply proportional to the spin-wave cross section, given by Eqs. (77),(79). Indeed, the ellipsoid of the triple axis spectrometer performs a 2D integration over in-plane (q_a,q_b) wave vectors. The measured intensity is then proportional to the 2D integrated spin susceptibility,

$$\overline{S}(\mathbf{Q},\omega)=\int d^2qS(\mathbf{Q},\omega). \quad (80)$$

Since the neutron cross sections generally behave in an antiferromagnet as $\epsilon_q^{-1}\propto 1/q$ for low energies (but above

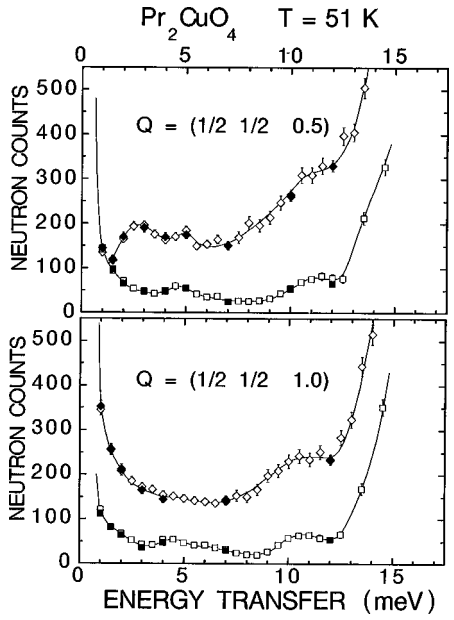

FIG. 7. Energy dependence of the measured neutron intensity in Pr_2CuO_4 at $T=51$ K at a zone boundary (upper panel) and a zone center (lower panel). Diamonds and squares correspond to intensity as measured, respectively, on the magnetic rod, $Q=(1/2,1/2,q_c)$, and out of rod, $Q=(h,h,q_c)$ with $h=0.42-0.44$ and $0.56-0.58$ (''background'') for the upper and lower panels, respectively. The filled symbols, corresponding to constant-energy scans across the magnetic rod, give more precise values of the background and of the magnetic scattering. Lines are guides through experimental points.

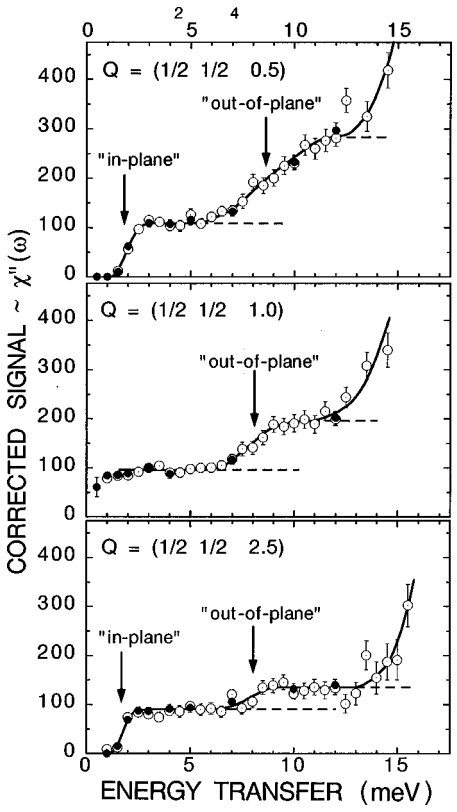

FIG. 8. Energy dependence of the magnetic signal divided by the thermal factor measured at different values of $q_c=0.5$, 1.0, and 2.5. The corrections of the signal taken from the data similar to Fig. 7 are made for the high-order scattering contribution to the incident beam monitor counts. The corrections are especially significant for the zone center ($q_c=1.0$) because the signal spreads to lower energies as compared to the zone boundaries ($q_c=0.5,2.5$). Lines are guides through experimental points. Arrows point to the positions of the observed energy gaps. Broken lines represent constant levels of the signal corresponding to each component of magnetic excitation spectrum.

gaps) [see, e.g., Eq. (79)], the 2D integration gives a result that is essentially energy independent apart from the temperature factor, $[1-\exp(-\omega/k_BT)]^{-1}$. Therefore, in an energy scan at constant wave vector, the measured intensity would increase when the energy enters the spin-wave dispersion surface and would then remain constant at higher energy (apart from the multiplicative temperature factor). This situation is sketched at $T=0$ on the right part of Fig. 6. The existence of a spin-wave branch having a minimum energy is thus detected as a step. This technique has been applied to investigate both the out-of-plane and the in-plane branches.

C. Thermal neutron experiment

On the thermal flux neutron spectrometer only the ''high''-energy part of the spectrum (energy transfer $\omega \geqslant 1$ meV) can be measured due to limitations of instrumental energy resolution. The typical neutron scattering spectra at $T=51$ K measured on the magnetic rod, i.e., for $\mathbf{Q}=(1/2,1/2,q_c)$, are depicted in Figs. 7 and 8. Similar data at $T=10$ K were reported in Ref. 14.

At the magnetic zone boundary, which corresponds to a semi-integer q_c, the obtained magnetic scattering signal reveals two steps corresponding to energy transfers of ~ 2 meV and $\sim 8-9$ meV (Fig. 8). The higher energy step becomes practically indistinguishable at large values of scattered wave vectors ($q_c>2.5$) while the lower one survives even at those values of q_c.

Such dependences on scattered wave vector manifest the ''in-plane'' polarization of the excitations that appear just above 2 meV in contrast to the ''out-of-plane'' polarization of the other component of magnetic intensity coming up with the second energy step. The different behavior of the in-plane and the out-of-plane components of the scattered intensity is explained by the geometrical factor in magnetic neutron scattering cross section [see Eqs. (77) and (79)], implying a suppression of the fluctuations polarized along the scattered wave vector. This means that at large q_c, when $\mathbf{Q}$ is getting more and more perpendicular to the basis plane of the crystal lattice, the out-of-plane (or the tetragonal axis polarized) component diminishes while there is always a contribution from the in-plane component. In addition, the magnetic form factor of copper ions controls the continuous decrease of magnetic scattering intensity at larger $\mathbf{Q}$; thus small values of q_c are preferably chosen for neutron scattering measurements.

Qualitatively, the observed energy and wave-vector dependence of the magnetic signal at the magnetic zone boundary correspond to that of Nd_2CuO_4.[14] The remarkable difference is the large width of the higher-energy step in the case of Pr_2CuO_4, which is significantly broader than the instrumental resolution. This could signify an essential

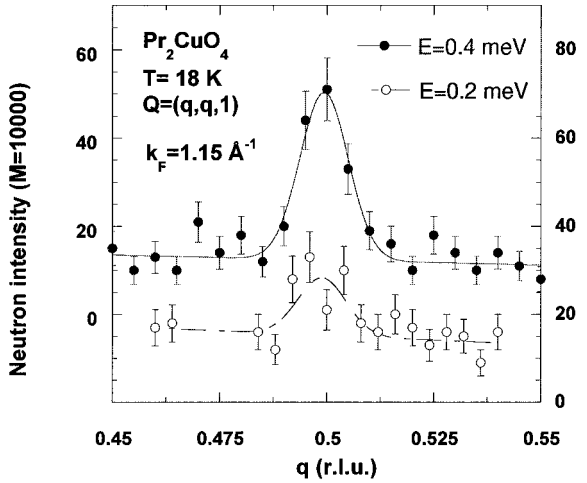

FIG. 9. Q scans along the $(qq1)$ direction for two fixed energy transfers: open circles at $\hbar\omega=0.2$ meV (right scale) and closed circles at $\hbar\omega=0.4$ meV (left scale). Lines are fit by the Gaussian.

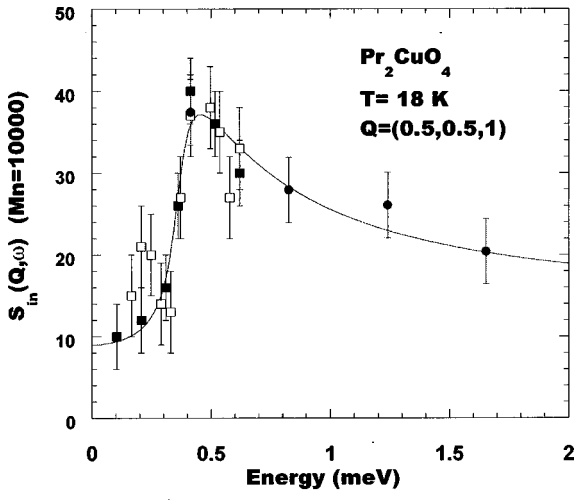

FIG. 10. In-plane scattering functions at the AF wave vector $Q=(0.5,0.5,1)$. Measurements performed using different experimental conditions (i) fixed $k_F=1.15$ Å^{-1} (squares) and (ii) fixed $k_I=1.55$ Å^{-1} (circles) have been rescaled. Closed symbols have been obtained from q scans (see Fig. 9). Open squares have been obtained from energy scan at the AF wave vector where the background has been subtracted. The line is a fit of Eq. (79) convoluted with the resolution function and small damping is included (see text).

damping of the out-of-plane excitations in Pr-copper oxide with presently unclear origin. On the other hand, the determination of the value of the out-of-plane energy gap is complicated by the presence of the strong background above ~ 12 meV energy transfer (Fig. 8) and essential increase of the intensity of the ''on-rod'' signal in this energy range (Fig. 7). Our measurements show that such an increase, which was not observed in Nd_2CuO_4,[14] could be related to the effect of the interaction between copper spin waves and the 18-meV crystal-field excitation of the Pr ions.[1]

We mention that the appearance of the out-of-plane spin fluctuation component in Pr_2CuO_4 was inscribed in Ref. 1 to an observed energy step at ~ 5 meV at the temperature of 10 K and it was claimed that it is a value of the out-of-plane spin-wave gap. Our data on Pr-copper oxide taken at different temperatures between 1.8 and 51 K, including those at $T=10$ K (see Ref. 14), do not show remarkable temperature dependence of the out-of-plane energy gap, which is equal to 8.5 ± 0.5 meV. Comparing the experimental conditions of the two experiments we claim that our data are taken with a better contrast, i.e., ratio of magnetic signal to nonmagnetic background, and with much better statistical accuracy than in Ref. 1.

In Nd_2CuO_4, a qualitatively different behavior from Pr_2CuO_4 is observed at the magnetic zone center $(q_c=1)$. Indeed, as pointed out in Ref. 14, in Nd_2CuO_4 both the in-plane and out-of-plane spin fluctuation components did not show measurable q_c dependence of the corresponding energy gaps. In the case of Pr_2CuO_4, only the out-of-plane energy gap remains largely unchanged as compared to the zone boundary scans along c, while the intensity of scattering from low-frequency in-plane polarized magnetic fluctuations drastically changes (Fig. 7). Now in the accessible energy range we do not see a clear step signifying an energy gap down to at least 1 meV energy transfer (Fig. 8). One can conclude that the in-plane component of magnetic fluctuations in Pr_2CuO_4 exhibits a certain dispersion that is not present in the case of the brother compound Nd_2CuO_4 and that evidently develops in the low-energy scale $\omega \leqslant 3$ meV. This energy range, which corresponds to essential changes of the in-plane copper spin fluctuations in Pr_2CuO_4, is discussed in more detail below.

D. Cold neutron experiment

We now present the low energy results (below 4 meV) where only the in-plane spin components occur. In contrast to the out-of-plane component, the in-plane one exhibits a clear dispersion. We first show the experimental evidence of an in-plane gap that appears as a result of the breaking of the rotational invariance in the (a,b) plane. Figure 9 displays q scans across the magnetic rod at the AF Bragg wave vector $Q=(0.5,0.5,1)$. At $\omega=0.4$ meV, a magnetic signal centered around $q=0.5$ is sizeable above a flat background. At lower energy, here at $\omega=0.2$ meV, this signal is clearly reduced. This demonstrates the existence of small energy gap of the spin excitations spectrum. Figure 10 depicts the peak intensity versus energy at 18 K. It corresponds to the in-plane scattering function, $\overline{S_{in}}(\mathbf{Q},\omega)$ [see Eq. (80)], which exhibits an asymmetric maximum at 0.4 meV. Here, the thermal population factor enhances the lower energy excitations leading to the observed asymmetric shape. A similar result for $q_c=1.7$ is shown in Fig. 11, where two clear steps are observed. These steps correspond to an acoustic and an optical excitation [see Eqs. (60)]. We have repeated such measurements for several representative values of q_c and obtained the results plotted in Fig. 12. A clear dispersion along the AF line is observed for both acoustic and optical branches. For wave vectors corresponding to integer value of q_c, a small gap is always visible demonstrating the breakdown of the rotation invariance in the (a,b) tetragonal plane with easy directions along a and b axes. At $q_c=0$, no point is reported below 2.5 meV because no magnetic scattering is sizeable at

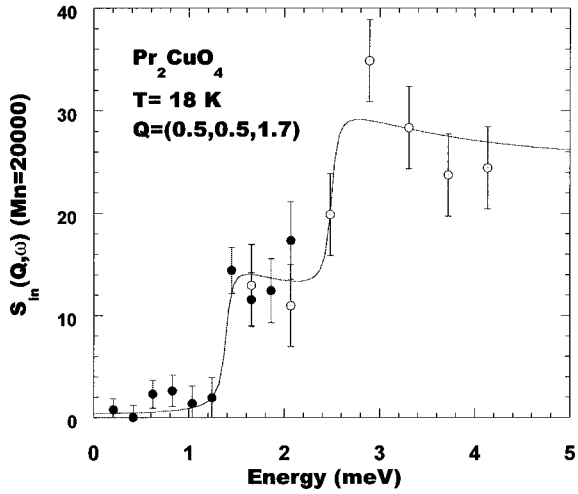

FIG. 11. In-plane scattering functions at the wave vector $Q=(0.5,0.5,1.7)$. Measurements performed using different experimental conditions (i) fixed $k_F=1.55$ Å^{-1} (open circles) and (ii) fixed $k_I=1.55$ Å^{-1} (closed circles) have been rescaled. All points have been obtained from q scans. The line is a fit of Eq. (79) convoluted with the resolution function.

low energy. This vanishing of the low-energy scattering for $q_c=0$ is confirmed in the upper part of Fig. 13. This scan has been performed along the AF line for an energy transfer of 0.6 meV as sketched by the dashed arrow in Fig. 12. It then crosses the acoustic dispersion curves near integer values of q_c yielding observed peaks. However, at $q_c=0$, the acoustic excitation is not observed.

In order to describe further these results, we now consider theoretical expressions for the spin-wave neutron cross sections for the in-plane component given in the preceding section. In the case of Pr_2CuO_4, the structure is of La_2NiO_4 type with $t=1$ in Eq. (79). The magnetic scattering is maximal along wave vectors $\mathbf{Q}=(0.5,0.5,q_c)$ for which $\cos(\mathbf{Q}\cdot\boldsymbol{\delta})=-\cos(\pi q_c)$. The in-plane scattering function can then be written as

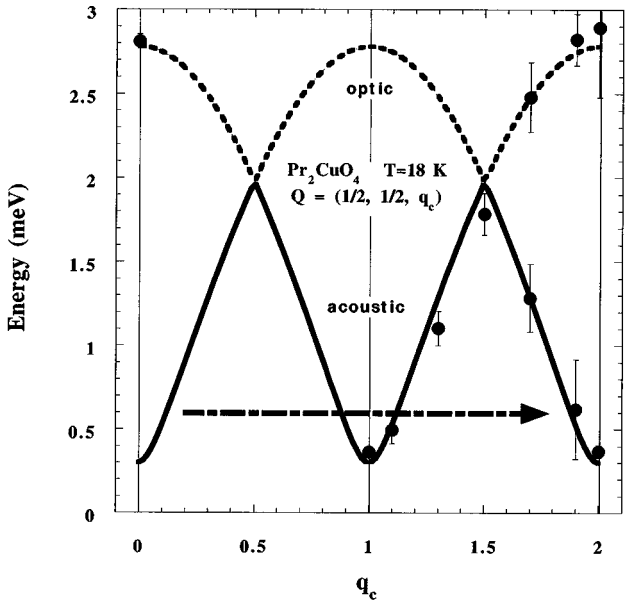

FIG. 12. In-plane spin components dispersion curves along the c^* direction. The arrow indicates the path of the scan reported in Fig. 13. Lines are fit to Eqs. (60), corresponding to low-energy acoustic (full line) and high-energy optical (dashed line) excitations, respectively.

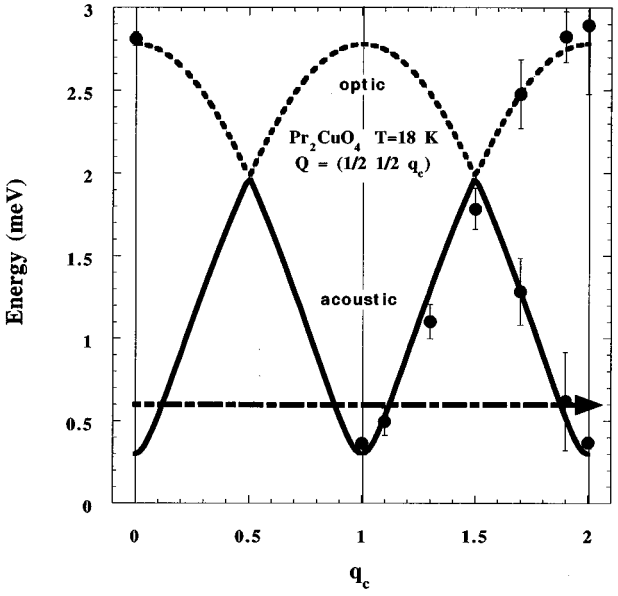

FIG. 13. Upper part: Q scan along the c^* axis at a fixed small energy transfer. The spin-wave scattering persists near all integer q_c except at $q_c=0$. The line is a guide to the eye. Lower part: dynamical structure factor for in-plane spin components for acoustic (full line) and optical excitations (dashed line) where according to the suggestion below Eq. (78) we refer to as acoustic and optical the branches with plus and minus sign in Eqs. (60) for all q_c. The atomic form factor of copper spins, $F(Q)$, has been included for comparison with the experimental result. We note the absence of any scattering on the acoustic branch at $q_c=0$ due to the interference effect discussed in the text.

$$S_{in}(\vec{Q},\omega)=\frac{S^2J_0}{2[1-\exp(-\omega/k_BT)]}\times\left\{\frac{A_{opt}}{\epsilon_{opt}}\delta(\omega-\epsilon_{opt})+\frac{A_{ac}}{\epsilon_{ac}}\delta(\omega-\epsilon_{ac})\right\},\tag{81}$$

where $A_{ac,opt}=1+Q_c^2/Q^2\mp(1-Q_c^2/Q^2)\cos(\pi q_c)$ where the signs $(-)$ and $(+)$ stand for the acoustic and optical branches, respectively, and $Q_c=(2\pi/c)q_c$. Let us notice that the factor $\delta(\omega-\epsilon_{ac,opt})/\epsilon_{ac,opt}$ is usual for antiferromagnetic spin-wave cross sections whereas the $A_{ac,opt}$ terms result from the noncollinear spin structure. This expression, when convoluted with the spectrometer resolution, can describe the measured in-plane scattering functions. It accounts very well for its observed shape and lines in Figs. 10 and 11 represent the best fits. In this expression, no damping is included due to the sharpness of the steps, which corresponds to the energy resolution. However, at $q_c=1$ (Fig. 10) a weak magnetic scattering extends up to the lowest energy investigated ($\omega=0.1$ meV). As a matter of fact, one can account for this tail by including a damping of about 0.2 meV into Eq. (81).

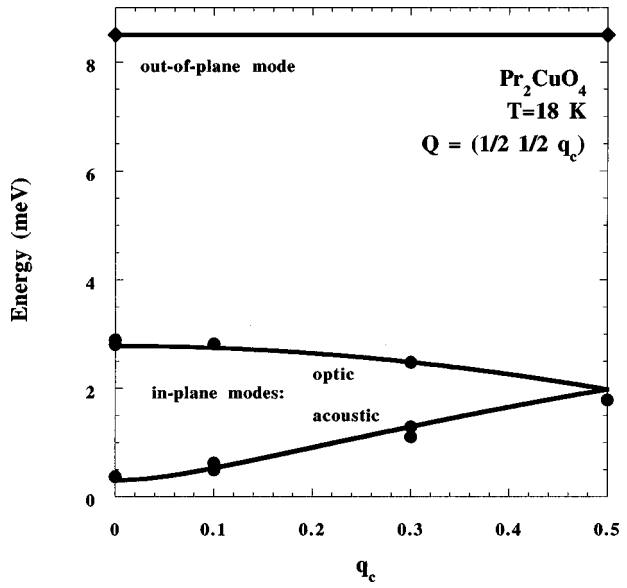

FIG. 14. Spin-wave dispersion curves along the c^* direction in noncollinear Pr_2CuO_2. The lines are fit by Eqs. (60) and (61) for the in-plane and the out-of-plane excitations, respectively.

The $A_{ac,opt}$ terms are reported in the lower part of Fig. 13: they display striking interference effect. The lower-energy branch (acoustic excitations) has a structure factor given by the full line: clearly, for $q_c=0$, the acoustic scattering is forbidden. This exactly explains the observed q_c dependence (upper part in Fig. 13). Thus our model with pseudodipolar interactions in noncollinear spin structure satisfactorily explains the vanishing of the acoustic mode structure factor at $q_c=0$.

E. Determination of the magnetic interactions

We now deduce magnetic parameters: (i) the pseudodipolar intraplane interaction P responsible for the in-plane gap, (ii) the pseudodipolar interplane interaction Q responsible for the dispersion along the c^* axis, (iii) the planar XY anisotropy A related to the out-of-plane gap. Figure 14 resumes the whole dispersion scheme along c^* axis within the first magnetic Brillouin zone. The two in-plane components and the twice degenerated out-of-plane component are presented. The out-of-plane branch does not depend on q_c and the out-of-plane gap, which is found to be at $\Delta_{out}=8.5\pm0.5$ meV at 10 K. It is a larger value than the one previously reported.[1] As we have pointed above, our data are taken with much better statistical accuracy than in Ref. 1 and thus we believe that they are more reliable. The in-plane spin component exhibits clear dispersion along c^*. Lines in Fig. 14 as well as dashed and full lines in Fig. 12 correspond to the calculated dispersion on the basis of Eqs. (60) with $I=0$. Clearly, description in terms of pseudodipolar interactions only reproduces very accurately the observed dispersion. Having in mind the discussion after Eq. (8) we conclude that the pseudodipolar interaction between neighboring planes Q is the interaction responsible for the observed 3D long-range magnetic order and one does not need to consider the interaction I between copper spins along the $\hat{c}$ axis.

From the measurements at integer values $q_c=1$ and 2, we obtain a value of $\Delta_0=0.36\pm0.03$ meV for the lowest gap of the in-plane excitations at $T=18$ K. Applying Eq. (40) for $S=1/2$, we obtain $P=0.45\pm0.04$ meV for the intraplane pseudodipolar interaction. This value is one order of magnitude larger than the value theoretically estimated in Refs. 22 and 23. Furthermore, this value is confirmed by an analysis of the spin-flop transition data of Ref. 1 given below in Sec. VII as well as the AFR data.[34] We discuss this problem in the last section of this paper.

According to Eqs. (60) and (61) all other spin-wave parameters depend on the strong in-plane nearest-neighbor superexchange interaction J. Hence, in order to determine these magnetic interactions, a precise value of J is required.

Knowing the spin-wave velocity c_0 one can determine J using renormalized spin-wave energy (53) where $\epsilon_{\mathbf{k}}=2SJ\sqrt{2}ka$ and a is the lattice constant. Corresponding values given in Ref. 1 are follows: $c_0=0.85\pm0.08$ eV Å and $J=130\pm13$ meV. Recent, more precise experiments based on the localization effect in the momentum space for Pr_2CuO_4 gave $c_0=0.81\pm0.02$ eV Å and $J=124\pm3$ meV.[35] Our results only slightly depend on the difference in J values given in Refs. 1 and 35. However, below we will use the last one.

From our experimental data and Eqs. (60) with $I=0$, the total amplitude for the dispersion is $\sqrt{16SJR_0}=2.8\pm0.05$ meV, and for $S=1/2$, one obtains $R_0=7.9\pm0.05\times10^{-3}$ meV. Then, using the determination of R_0 given by Eq. (24) and the lattice constants $a=3.958$ Å and $c=12.19$ Å, we get the interplane pseudodipolar constant as $Q=0.023\pm0.001$ meV. This value is one order of magnitude larger than the corresponding dipolar magnetic interactions (see last section). From the out-of-plane gap, $\Delta_{out}=8.5\pm0.5$ meV given above and Eq. (61) we get $A=[6.9\pm0.5\times10^{-2}](S/\langle S\rangle)^2$ meV and using the experimental value of the ratio $\langle S\rangle/S=0.8$[1] we obtain $A=(10.8\pm0.1)\times10^{-2}$ meV. This value of the easy-plane anisotropy is three times larger than that discussed in Refs. 22 and 23.

We compare now these results for Pr_2CuO_4 with available data for Nd_2CuO_4 and point out the following striking differences. (i) In Nd_2CuO_4 there are two spin reorientation transitions at $T_1\simeq80$ K and $T_2\simeq30$ K (Refs. 2,3,10) [see Fig. 1(b)]. It means that the interplane PD interaction Q changes sign twice.[19] (ii) Both in-plane and out-of-plane gaps are strongly T dependent and the former is one order of magnitude larger than in the case of Pr_2CuO_4. (iii) The dispersion of the in-plane excitations along the $(1/2,1/2,q_c)$ direction has not been observed.[14]

The first and the second peculiarities are related to the Kramers ground state of the Nd^{3+} ions and will be discussed in Sec. IX. The latter may be explained by the large value of the in-plane gap. Indeed, in this case from Eqs. (60) with $I=0$ we obtain the following extremal values of the in-plane spin-wave energy:

$$\epsilon_{in}^{(\max)}\simeq\Delta_0+\frac{8SJR_0}{\Delta_0},\qquad \epsilon_{in}^{(\min)}=\Delta_0. \tag{82}$$

According to Ref. 14 the smaller value of Δ_0 is approximately 2.5 meV at high temperature and the experimental error is ±0.25 meV. Hence, the dispersion cannot be visible

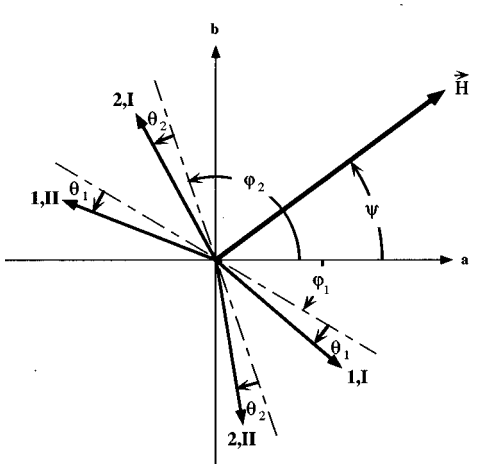

FIG. 15. Spin configuration in magnetic field. Indices (1I),(1II) and (2I),(2II) label neighboring spins I and II in the subsystems 1 and 2, respectively.

if $(16SJR_0)^{1/2} \leqslant 1.6$ meV, i.e., the same order of magnitude as determined above for Pr_2CuO_4.

VII. SPIN CONFIGURATION IN MAGNETIC FIELD

In this section we examine the copper spin configuration of the noncollinear AF R_2CuO_4 in magnetic field applied in the basal plane at $T=0$. We obtain the corresponding expression for the ground-state energy and analyze it in two practically important limiting cases studied in Refs. 1–5: (i) **H** along the [1,1,0] direction and (ii) **H** at small angle to the a (b) axis. We demonstrate that in the former case the transition is second order, with a critical field given by Eq. (2).

The spin configuration in magnetic field is shown in Fig. 15. At the first sign we obtain the ground-state energy of the system adding to Eq. (41) terms that describe a change of the energy connected with relative rotations of the sublattices on the angles ϑ_1 and ϑ_2 in the corresponding perpendicular magnetic fields (see Fig. 15 and Appendix A). These terms are given by

$$\Delta E_{1,2}=S^2J_0N\left[\left(\vartheta_{1,2}+\frac{g\mu H_{\perp,1,2}}{2SJ_0}\right)^2-\left(\frac{g\mu H_{\perp,1,2}}{2SJ_0}\right)^2\right], \tag{83}$$

where $H_{\perp,1,2}=H\sin(\psi-\varphi_{1,2})$ and $\vartheta_{1,2}\ll 1$. As is well known (see also Appendix A), at equilibrium we have

$$\vartheta_{1,2}=-\vartheta_{01,2}=-\frac{g\mu H_{\perp,1,2}}{2SJ_0},$$
$$\Delta E_{1,2}=-S^2J_0N\left(\frac{g\mu H_{\perp 1,2}}{2SJ_0}\right)^2. \tag{84}$$

However, rotations of sublattices on angles $\vartheta_{1,2}$ give rise to simultaneous rotations of the corresponding y axes and an additional interaction appears between y spin components and magnetic field. This interaction is linear in operators $(a_0-a_0^+)/i$ and $(a_{\mathbf{k_0}}-a_{\mathbf{k_0}}^+)/i$. It should be excluded as well as the interaction W_1 given by Eq. (21). It was done in Appendix A. As a result we have Bose condensation of the in-plane spin waves with $\mathbf{k}=0$ and $\mathbf{k}=\mathbf{k}_0$, the ground-state energy acquires an additional term and is represented as follows:

$$\begin{aligned}E=S^2NJ_0\Bigg[&\frac{\Delta_0^2}{16(SJ_0)^2}(\sin^2 2\varphi_1+\sin^2 2\varphi_2)\\&-\left(\frac{g\mu H_{\perp,1}}{2SJ_0}\right)^2-\left(\frac{g\mu H_{\perp,2}}{2SJ_0}\right)^2-\frac{R_0}{SJ_0}\Bigg]\\&-S^2NJ_0\{X_1^2[\Delta_{in,2}^2+2SJ_0R_0-(g\mu H_{\parallel,2})^2]\\&+X_2^2[\Delta_{in,1}^2+2SJ_0R_0-(g\mu H_{\parallel,1}^2)]-4SJ_0R_0X_1X_2\}\\&\times\{[\Delta_{in,1}^2+2SJ_0R_0-(g\mu H_{\parallel,1})^2]\\&\times[\Delta_{in,2}^2+2SJ_0R_0-(g\mu H_{\parallel,2})^2]-(2SJ_0R_0)^2\}^{-1},\end{aligned} \tag{85}$$

where R_0 is given by Eq. (24) and

$$\Delta_{in,1,2}^2=\Delta_0^2\cos 4\varphi_{1,2}+(g\mu H_{\perp,1,2})^2,$$
$$X_{1,2}=SQ_{\mathbf{k}_0}\cos(\varphi_1+\varphi_2)+(g\mu H_{\perp 1,2})(g\mu H_{\parallel 1,2})/(2SJ_0). \tag{86}$$

The minimum of this energy as a function of φ_1 and φ_2 determines the ground-state spin configuration. If $g\mu H \ll \Delta_0$ the last term in Eq. (85) is small and may be neglected. In the end of Appendix B we will show that the denominator of this term is a squared product of the in-plane spin-wave energies at $\mathbf{k}=0$. As is well known the spin-flop transition takes place when one of the spin-wave branches becomes gapless. Hence, near the transition this denominator is small and the second term in Eq. (85) becomes essential.

If we neglect the interplane PD interaction, the energy E becomes a sum of two terms corresponding to independent subsystems 1 and 2. In particular, the ground-state energy of conventional two-sublattice tetragonal antiferromagnets is determined by

$$E=S^2NJ_0\left\{\frac{\Delta_0^2}{16(SJ_0)^2}\sin^2 2\varphi-\left(\frac{g\mu H_\perp}{2SJ_0}\right)^2-\frac{(g\mu H_\perp g\mu H_\parallel)^2}{(2SJ_0)^2[\Delta_{in}^2-(g\mu H_\parallel)^2]}\right\} \tag{87}$$

if $\hat{a}(\hat{b})$ is an easy axis. According to the end of Sec. V the same expression remains valid for the [1,1,0] easy direction if one changes the sign in front of Δ_0^2 in Eqs. (86) and (87).

It should be noted also that Eq. (87) is applicable to the AF compound $YBa_2Cu_3O_{6+x}$ (YBCO) with antiferromagnetically coupled adjacent planes (CuO_2 bilayers). Indeed in magnetic-field neighboring spins along $\hat{c}$ axis rotate in opposite directions without violation their mutual antiparallel orientation. Hence experimental studies similar to Refs. 1–5 provide a possibility to determine magnetic anisotropy of undoped YBCO compound as well as the value of the in-plane spin-wave gap. It has been done recently.[36]

Let us consider now the ground-state spin configuration in two important limiting cases that have been studied

experimentally.[1–5] (1) The field is along the [1,1,0] direction ($\psi=\pi/4$). (2) Field is applied at the angle $\psi \ll 1$ of the [1,0,0] direction.

We begin with the case $\psi=\pi/4$. Due to the symmetry the spins of two subsystems rotate in opposite directions by the same angle $\varphi=\varphi_1$, the sum $\varphi_1+\varphi_2$ remains unchanged and R_0 is a constant. As a result from Eqs. (85) and (86) we get

$$E=2S^2NJ_0\left\{\frac{\Delta_0^2}{16(SJ_0)^2}\sin^2 2\varphi-\left(\frac{g\mu H}{2SJ_0}\right)^2\sin^2\left(\frac{\pi}{4}-\varphi\right)\right.$$
$$\left.-\frac{(g\mu H)^4\cos^2 2\varphi}{4(2SJ_0)^2[\Delta_0^2\cos 4\varphi-(g\mu H)^2\sin 2\varphi]}\right\}. \quad (88)$$

This energy differs by the factor 2 only from the energy of the collinear system given by Eq. (87). Hence, the subsequent analysis is applicable to both collinear and noncollinear systems. It is a result of a particular symmetry of the problem at $\psi=\pi/4$.

For small field, one can neglect the second term in Eq. (88) and obtain

$$\sin 2\varphi=-\left(\frac{g\mu H}{\Delta_0}\right)^2. \quad (89)$$

This field dependence of $\sin 2\varphi$ has been used in Ref. 5 for description low-temperature neutron scattering data in Pr_2CuO_4. From Eq. (89) we get also Eq. (2) for the critical field of the transition. However, at $\sin 2\varphi=-1$ the denominator in the second term of Eq. (88) is equal to zero and the problem needs more careful consideration.

Let us rewrite Eq. (88) in the following form:

$$\frac{E}{2S^2J_0N}=-h^2+\frac{\delta^2}{4}\cos^2 2\alpha-\tfrac{1}{2}h^2\cos 2\alpha$$
$$-\frac{h^4\sin^2 2\alpha}{4(-\delta^2\cos 4\alpha+h^2\cos 2\alpha)}, \quad (90)$$

where $\alpha=\varphi+\pi/4$, $\delta=\Delta_0/(2SJ_0)$ and $h=g\mu H/(2SJ_0)$. From the condition $dE/d\alpha=0$ we get

$$\left[(-\delta^2\cos 2\alpha+h^2)Z^2-h^4Z\cos 2\alpha\right.$$
$$\left.+\frac{h^4}{2}\sin 2\alpha(2\delta^2\sin 4\alpha-h^2\sin 2\alpha)\right]\sin 2\alpha=0, \quad (91)$$

where $Z=-\delta^2\cos 4\alpha+h^2\cos 2\alpha$. The solution $\alpha=0$ corresponds to the collinear state.

If $h^2\ll\delta^2$ we can take into account the first term only, which gives Eq. (89) again. In the near transition region where $\delta^2-h^2\ll\delta^2$ and $\alpha\ll 1$ we obtain after simple calculations

$$\alpha=\left\{\frac{\Delta_0^2-(g\mu H)^2}{2\Delta_0^2}\right\}^{1/4}\simeq\left(\frac{\Delta_0-g\mu H}{\Delta_0}\right)^{1/4} \quad (92)$$

instead of $\alpha=\{[\Delta_0^2-(g\mu H)^2]/(2\Delta_0)^2\}^{1/2}\simeq[(\Delta_0-g\mu H)/\Delta_0]^{1/2}$, which follows from Eq. (89). This crossover from $\alpha\sim(\Delta_0-g\mu H)^{1/2}$ to $\alpha\sim(\Delta_0-g\mu H)^{1/4}$ behavior near the transition has been observed recently in Pr_2CuO_4.[28] It should be noted that Eq. (92) is not applicable at the very vicinity of the transition where the critical fluctuations become important [see discussion in Appendix A after Eq. (A.21)].

We consider now the case of the field directed almost along $\hat{a}$ axis, i.e., when $\psi\ll 1$. It is the case, studied experimentally in Refs. 3 and 4. If $\psi=0$ the second term in Eq. (85) disappears. However the spin-flop field may be determined from the condition of the positiveness of the denominator (see Appendix B). As a result for $\psi=0$ we get

$$g\mu H_c=[\Delta_0^2(\Delta_0^2+4SJ_0R_0)]^{1/4}. \quad (93)$$

Obviously, the spin-flop transition is of the first-order one and if $H>H_c$ we have the state with all spins along $\hat{b}$ direction.

If $\psi\ll 1$, for small field we can neglect the second term in Eq. (85) and obtain for the ground-state energy the following expression:

$$E=S^2NJ_0\left\{\frac{\Delta_0^2}{16(SJ_0)^2}(\sin^2 2\varphi+\sin^2 2\eta)-\frac{8|Q_0|}{J_0}\cos(\varphi+\eta)\right.$$
$$\left.-\left(\frac{g\mu H}{2SJ_0}\right)^2[\sin^2(\psi-\varphi)+\cos^2(\psi-\eta)]\right\}, \quad (94)$$

where $\varphi=\varphi_1$, $\eta=\varphi_2\mp\pi/2$, and we used the definition (24) for R_0. The energy E depends now on two independent variables, and from the conditions $\partial E/\partial\varphi=\partial E/\partial\eta=0$ we have

$$\varphi=-\frac{(g\mu H)^2(\Delta_0^2+24S^2J_0|Q_0|)\psi}{\Delta_0^2(\Delta_0^2+32S^2J_0|Q_0|)}\simeq-\frac{3(g\mu H)^2}{4\Delta_0^2}\psi, \quad (95)$$

$$\eta=\frac{(g\mu H)^2(\Delta_0^2+48S^2J_0|Q_0|)\psi}{2\Delta_0^2(\Delta_0^2+32S^2J_0|Q_0|)}\simeq\frac{3(g\mu H)^2}{4\Delta_0^2}\psi. \quad (96)$$

We see that φ and η are proportional to the angle ψ in agreement with experimental data of Ref. 3 and $\varphi+\eta\simeq 0$ if $\Delta_0^2\ll 8S^2J_0|Q_0|$. With increasing ψ the spin flop remains the first-order transition and smoothly approaches the second-order one at $\psi=\pi/4$.

Using Eq. (2) and data of Ref. 1 one can determine the in-plane spin-wave gap for Pr_2CuO_4 independently from the inelastic scattering. Indeed from Fig. 4 Ref. 1 we obtain the critical field $H_c=4.4T$ at 4.2 K and $\Delta_0=0.51$ meV, if $g=2$. This value is slightly larger than $\Delta_0=0.36\pm0.03$ meV given above. However, from the same figure we get $H_c=2.0T$ and $\Delta_0=0.23$ meV at $T=25$ K. Assuming linear T dependence of H_c we obtain $\Delta_0=0.33$ meV at $T=18$ K in satisfactory agreement with inelastic scattering data. However, we need to be careful about this comparison as the samples used in Ref. 1 and this study have different Néel temperatures: $T_N=284$ K and $T_N=247$ K, respectively. In this respect we wish to point out that, in a sample with $T_N=249$ K, a reentrant behavior of H_c has been observed with

a maximum at $T_m \simeq 5$ K.[28] Nevertheless, the observed T dependence of the critical field H_c is actually confirmed by preliminary inelastic neutron scattering, which indicates a similar T dependence at low temperature (below ~ 20 K). Although its theoretical explanation is still unclear, it is probably related to the interactions between spin waves.

Hence, we conclude that the data of Ref. 1 confirm the large value of the in-plane gap in comparison with the theoretical calculations of Refs. 22 and 23. Interestingly, it should be emphasized that, in the undoped YBCO compound, a similar value $\Delta_0 \simeq 0.3$ meV has been recently deduced from the field dependence of the AF Bragg intensity.[36]

VIII. SPIN-WAVE SPECTRUM IN MAGNETIC FIELD AND INELASTIC NEUTRON SCATTERING

Similarly to the above discussion we restrict ourselves to consideration of the spin-wave spectrum in magnetic field along the $\hat{c}$ direction only, when $k_a = k_b = 0$. The spin-wave modes are the solutions of the equation $Z(\omega) = 0$, where Z is given by Eq. (B12). In the considered case, it may be represented as follows:

$$d_1(\omega) d_2(\omega) - \left[2SJ_0 R_0 \cos\frac{k_c}{2} \right]^2 [\omega^2 - \Delta_{out}^2 + (g\mu H_{\parallel 1})^2] \times [\omega^2 - \Delta_{out}^2 + (g\mu H_{\parallel 2})^2] = 0, \quad (97)$$

where Δ_{out}^2 is given by Eq. (61) and

$$d_{1,2}(\omega) = (\omega^2 - \Delta_{out}^2)(\omega_1^2 - \epsilon_{1,2}^2) - (g\mu H_{\parallel 1,2})^2 \times (2\omega^2 + \Delta_{out}^2 + \epsilon_{1,2}^2) + (g\mu H_{\parallel 1,2})^4, \quad (98)$$

$$\epsilon_{1,2}^2 = \Delta_0^2 \cos 4\varphi_{1,2} + (g\mu H_{\perp 1,2})^2 + 2SJ_0 R_0 .$$

At $H = 0$ from (97) we get Eqs. (60) and (61).

As we will see below in real systems such as Pr_2CuO_4 the out-of-plane gap Δ_{out}^2 is much larger than Δ_0^2, $2SJ_0R_0$, and $g\mu H \lesssim \Delta_0$. Hence, the field corrections to the out-of-plane mode are negligibly small. At the same time for evaluation of the in-plane modes we may neglect $(g\mu H_{\parallel})^2$ and ω^2 comparing with Δ_{out}^2. As a result, instead of Eq. (97) we get

$$[\omega^2 - \epsilon_1^2 + (g\mu H_{\parallel 1})^2][\omega^2 - \epsilon_2^2 + (g\mu H_{\parallel 2})^2] - \left[2SJ_0 R_0 \cos\frac{k_c}{2} \right]^2 = 0. \quad (99)$$

The solution of this equation is given by

$$\epsilon_{\pm}^2 = \frac{1}{2}[\epsilon_1^2 + \epsilon_2^2 - (g\mu H_{\parallel 1})^2 - (g\mu H_{\parallel 2})^2] \pm \frac{1}{2}\left\{ [\epsilon_1^2 - \epsilon_2^2 + (g\mu H_{\parallel 2})^2 - (g\mu H_{\parallel 1})^2]^2 + 4\left[2SJ_0 R_0 \cos\frac{k_c}{2} \right]^2 \right\}^{1/2}. \quad (100)$$

As in the previous section we consider the two cases $\psi = 0$ and $\psi = \pi/4$.

a. $\psi = 0$. Below the spin-flop transition where $g\mu H < \Delta_0$ the spin structure is determined by angles $\varphi_1 = 0$ and $\varphi_2 = \pm \pi/2$. In this case, instead of Eq. (60), we have

$$\epsilon_{\pm}^2 = \Delta_0^2 + 2SJ_0 R_0 + 4S^2 J_0 I(1 - \cos k_c) \pm \left\{ \left[2SJ_0 R_0 \cos\frac{k_c}{2} \right]^2 + (g\mu H)^4 \right\}^{1/2}. \quad (101)$$

We see that now there is a gap at $k_c = \pi$ equal to $(g\mu H)^2 (\Delta_0^2 + 2SJ_0 R_0)^{-1/2}$ if $I = 0$ between acoustic and optical branches. At the same time the spin-flop field is determined by the condition $\epsilon_-^2(k_c = 0) = 0$, which coincides with Eq. (93). In the spin-flop phase we have $\varphi_1 = -\pi/2$, $\varphi_2 = \pm \pi/2$ and $R_0 = 0$ as $\varphi_1 + \varphi_2 = 0, \pi$, and we obtain the doubly degenerate in-plane mode with energy given by

$$\epsilon_{\mathbf{k}}^2 = \Delta_0^2 + (g\mu H)^2 + \epsilon_{\mathbf{k}R}^2 + 4S^2 J_0 I(1 - \cos k_c), \quad (102)$$

where $\epsilon_{\mathbf{k}R}^2$ is given by Eq. (53). We see that the spin-wave spectrum remains stable at all values of H, and, in particular, for $H < H_c$. It means that the metastable state should exist that may be achieved if after the spin-flop transition one lowers the field below H_c, as it should be in the case of the first-order transition. It should be noted also that Δ_0 in Eq. (102) may not coincide with the in-plane gap at $H = 0$ due to an additional contribution related to the Bose condensation of the uniform spin waves (see discussion in the end of Appendix A).

b. $\psi = \pi/4$. In this case two subsystems rotate in opposite directions at the same angle $\varphi = -\pi/2 + \alpha$ and R_0 remains constant. Near the transition where $g\mu H < \Delta_0$ the angle $\alpha = \pi/4 + \varphi$ is given by Eq. (92) and we obtain

$$\epsilon_{\pm}^2 = \{18\Delta_0^2[\Delta_0^2 - (g\mu H)^2]\}^{1/2} + 2SJ_0 R_0 \left[1 \pm \cos\frac{k_c}{2} \right] + 4S^2 J_0 I(1 - \cos k_c). \quad (103)$$

In the collinear phase we have $\varphi = -\pi/4$ and

$$\epsilon_{\pm}^2 = (g\mu H)^2 - \Delta_0^2 + 2SJ_0 R_0 \left[1 \pm \cos\frac{k_c}{2} \right] + 4S^2 J_0 I(1 - \cos k_c). \quad (104)$$

The ϵ_- mode is a gapless one exactly at the transition field $g\mu H = \Delta_0$ as it should be in the case of the second-order transition. However, due to critical fluctuations the field dependence of the gaps may deviate from the simple expressions given by Eqs. (103) and (104) [see discussion after Eq. (A.21)].

Let us consider now the neutron scattering by R_2CuO_4 systems in applied magnetic field. The elastic scattering has been discussed in Sec. IV. The out-of-plane spin-wave scattering remains unchanged [see Eq. (77)]. It may be easily shown using Eqs. (71) and (B18).

From Eqs. (72), (74), and (B10) for the scattering function S_{in} at $\omega > 0$ we get

$$S_{in}(\mathbf{Q},\omega)=\frac{S^2J_0}{1-e^{-\omega/k_BT}}\Bigg\{[\omega^2-\epsilon_2^2+(g\mu H_{\|2})^2]\left(1-\frac{Q_{y1}^2}{Q^2}\right)+[\omega^2-\epsilon_1^2+(g\mu H_{\|1})^2]\times\left(1-\frac{Q_{y2}^2}{Q^2}\right)+4SJ_0(C-D)\times\left(\hat{e}_{y1}\hat{e}_{y2}-\frac{Q_{y1}Q_{y2}}{Q^2}\right)\cos(\boldsymbol{\tau}_{AF}\cdot\boldsymbol{\delta})\Bigg\}\times\left[\frac{1}{2\epsilon_+}\delta(\omega-\epsilon_+)-\frac{1}{2\epsilon_-}\delta(\omega-\epsilon_-)\right],\quad(105)$$

where $\epsilon_{1,2}^2$ is given by Eq. (98). As above we consider again two limiting cases $\psi=0$ and $\psi=\pi/4$.

a. $\psi=0$. We do not analyze here cumbersome expression for S_{in} below the spin-flop transition. Above this transition as well as in the metastable state below it we have $H_{\|\,1,2}=0$, $\epsilon_1=\epsilon_2=\epsilon_{\mathbf{k}}$, where $\epsilon_{\mathbf{k}}$ is given by Eq. (102) and we obtain

$$S_{in}(\mathbf{Q},\omega)=\frac{S^2J_0\delta(\omega-\epsilon_{\mathbf{k}})}{\epsilon_{\mathbf{k}}[1-\exp(-\epsilon_{\mathbf{k}}/k_BT)]}.\quad(106)$$

b. $\psi=\pi/4$. Again we do not analyze S_{in} below the transition. Above it we have collinear spin structure that coincides with the structure of La_2NiO_4 type at $t=1$ and La_2CuO_4 at $t=2$. For the scattering function we obtain

$$S_{in}^{(\pm)}=\frac{S^2J_0}{1-\exp(-\omega/k_BT)}\left(1-\frac{Q_{y1}^2}{Q^2}\right)\times[1\mp(-1)^t\cos(\boldsymbol{\tau}_{AF}\cdot\boldsymbol{\delta})]\frac{1}{2\epsilon_\pm}\delta(\omega-\epsilon_\pm).\quad(107)$$

We see that in this collinear structure the interplane interference remains and disappears if one neglects the interplane PD interaction. It should be noted that this interference is a consequence of a monodomain state after the transition. Indeed, in the applied field directions of the spin rotations are fixed [see Fig. 15] and as a result the monodomain state appears in contrast with the conventional collinear systems (see Ref. 3).

It should be noted also that in the considered case y_1 and y_2 axes are parallel to the field. As a result the intensity strongly depends on the projection of $\mathbf{Q}$ on the (a,b) plane. In particular if $\mathbf{Q}=(\frac{1}{2},-\frac{1}{2},0)$ we have $Q_{y1}^2/Q^2=1$ and the spin-wave scattering is forbidden. At the same time the scattering connected with the longitudinal z fluctuations is maximal. The intensity of this scattering calculated in the one-loop approximation displays the infrared divergence and $\mathrm{Im}\,\chi_{zz}$ in the gapless case at $\mathbf{Q}=\boldsymbol{\tau}+\mathbf{k}_0$ and $\omega\to0$ diverges as $1/\omega$ and T/ω^2 at $T=0$ and $T\neq0$, respectively.[37] Obviously this divergence should be screened by the higher-order terms. However, this very complex theoretical problem is far from the solution. It appears more demanded if one takes into account that similar infrared divergence appears in many other physical problems, such as the longitudinal spin fluctuations in ferromagnets with dipolar interaction.[38] Thus experimented investigation of the longitudinal fluctuations in the considered case is related to the important problem of the many-particle physics.

IX. RESULTS AND DISCUSSION

We investigated magnetic properties of noncollinear tetragonal antiferromagnets R_2CuO_4 with particular attention to Pr_2CuO_4 and Nd_2CuO_4. We obtain the following main results. (1) The noncollinear Cu^{2+} spin ordering below the Néel temperature is explained on the assumption of PD interaction between copper spins in CuO_2 planes as well as between the adjacent planes. Corresponding expression for the ground-state energy at $\mathbf{H}=0$ is given by Eq. (41). (2) We demonstrate that the interplane PD interaction contributes to the out-of-plane spin-wave gap [Eq. (61)] and splits the in-plane spin-wave mode into acoustic and optical branches [Eqs. (60)]. (3) Interaction between spin waves gives rise to the in-plane spin-wave gap, which depends on the orientation of the sublattice magnetization in the (ab) plane [see Eq. (59)]. This dependence is crucial for determination of the spin orientation in a magnetic field. In the end of Sec. IV it is shown that the φ dependence of the gap given by Eq. (59) is not a specific result connected to the PD interaction, but is actually a consequence of the square symmetry of CuO_2 planes. (4) We present the expressions for the neutron scattering cross sections, which take into account the noncollinear spin structure of the R_2CuO_4 compounds. (5) Detailed inelastic neutron scattering data are presented for Pr_2CuO_4 in the case of the transferred momentum along the $(1/2,1/2,q_c)$ direction. In particular, we demonstrate that acoustic spin-wave scattering is forbidden at $\mathbf{Q}=(1/2,1/2,0)$ due to destructive interference occurring in the noncollinear structure with pseudodipolar interactions. (6) We determine the out-of-plane spin-wave gap $\Delta_{out}=(8.5\pm0.5)$ meV. This value is larger than previously reported.[1] However, as shown in Sec. VI, our data are taken with much better statistical accuracy and our value of Δ_{out} is more reliable. (7) We observe acoustic and optical spin-wave branches and determine their dispersion (Fig. 14). It is well described by Eqs. (60). (8) From these data we determine that the in-plane spin-wave gap $\Delta_0=0.36\pm0.03$ meV and using Eq. (40) calculate the intraplane PD interaction $P=0.45\pm0.04$ meV. This value is one order of magnitude larger than the theoretically predicted in Ref. 22 and 23. However, it is confirmed by AFR (Ref. 34) and analysis of the transition data of Ref. 1 given in Sec. VII. Discussion of this disagreement is given below. (9) From the observed acoustic and optical branches we find a value of the interplane PD interaction $Q=[0.023\pm0.001]$ meV. This value is much larger than the corresponding magnetic dipolar interaction between neighboring Cu spins in the adjacent planes, which is given by

$$Q_{mag\text{-}dip}=-\frac{24(g\mu_B)^2}{[2a^2+c^2]^{3/2}}=-2.2\times10^{-3}\ \text{meV}\quad(108)$$

using the same definition as Q in Eq. (8). (10) The spin configuration of the noncollinear spin structure is analyzed in

magnetic field parallel to the (ab) plane. For the field along the [1,1,0] direction the transition is of second order and the critical field is given by Eq. (2). For other directions the transition is of first order. It is shown also that for the [1,0,0] direction the metastable spin-flop state should exist at $H < H_c$ where H_c is given by Eq. (93). (11) Analysis of the data of Ref. 1 confirms large value of the in-plane gap in Pr_2CuO_4 determined in the neutron scattering experiments. However, strong temperature dependence of the critical field H_c observed in Ref. 1 and confirmed in Ref. 28 remains unexplained. Presumably it is related to the nonlinear interaction between spin waves and canted magnetic field (see the end of Sec. VII). This interaction gives rise to a contribution to the free energy that is essential at $T > \Delta_0$. However, consideration of this problem is beyond the scope of this paper. (12) The spin-wave spectrum in magnetic field is considered and expressions for the inelastic neutron scattering cross sections are given.

The results listed above are discussed in the main part of the paper. Hence, here we present some additional comments. First of all, we wish to point out that the intraplane PD interaction maintains the long-range AF order at $T \neq 0$ in the isolated CuO_2 plane in contrast with the fact that in the linear theory the spin-wave spectrum is gapless and the spin deviation $S - \langle S \rangle$ diverges. Indeed, we have seen in Sec. IV that interaction between spin waves gives rise to the in-plane gap. By the same token the gap appears in the out-of-plane branch too, if $A = 0$. It has the following form:

$$\Delta_{out}^2 = \frac{SP^2}{(2\pi)^2} \int_{-\pi}^{\pi} dk_a dk_b \frac{(\cos k_a - \cos k_b)^2 [6 + 4(\cos k_a + \cos k_b)^2 - 7(\cos k_a + \cos k_b)]}{(2 - \cos k_a - \cos k_b)^{5/2} (2 + \cos k_a + \cos k_b)^{1/2}} \simeq 0.0334 SP^2. \quad (109)$$

These gaps Δ_{in} and Δ_{out} prevent the divergence of the spin deviation and maintain long-range magnetic order. Hence, we have a new example of the so-called ordering from the disorder (see Refs. 39 and 40 and references therein).

Comparison of the spin-wave gaps in Pr_2CuO_4 determined in this study and in Nd_2CuO_4 (Ref. 14) reveals the following important features. (i) The in-plane gap in Pr_2CuO_4, as well as in antiferromagnetic undoped YBCO compound,[36] is one order of magnitude less than in Nd_2CuO_4. (ii) In Nd_2CuO_4, both gaps are strongly T dependent, $\Delta_{in,out}^2 \sim 1/T$, whereas in Pr_2CuO_4 only the in-plane gap has a noticeable T dependence,[41] which is clearly different from the Nd-compound case. As a result we conclude that the values of both gaps are determined not only by the intrinsic properties of CuO_2 planes but also by the type of the RE ion. It may explain the difference of the value of the intraplane PD interaction determined above and calculated in Refs. 22 and 23. In particular, in addition to the intraplane PD interaction, the square anisotropy mediated by anisotropic interaction of the copper spins with RE ions in the form of Eq. (62) may contribute to the values of both gaps. In this respect it would be very important to determine the in-plane spin-wave gap in compounds without RE ions such as $Sr_2CuO_2Cl_2$ and the spin-flop experiments are urgent with magnetic field along the [1,1,0] and [1,0,0] directions. In this way one can find out if the magnetic structure of $Sr_2CuO_2Cl_2$ is noncollinear. In any case, Eq. (2) allows us to determine the in-plane gap. Indeed, this equation holds for $\mathbf{H} \| [1,1,0]$ and $\mathbf{H} \| [1,0,0]$ for the [1,0,0] and [1,1,0] easy axes, respectively.

As we have mentioned in the Introduction the Nd^{3+} crystal-field ground state is a Kramers doublet and its local susceptibility roughly behaves as $1/T$. It explains[9] spin reorientation transitions in Nd_2CuO_4 observed in Refs. 2, 3 and 10 (see Fig. 1). In Fig. 1(a), we see that there are two superexchange paths through one and two Nd ions, respectively, which connect neighboring Cu^{2+} ions in the adjacent planes. Corresponding contributions to the PD interaction between these ions are proportional $-Q_1/T$ and Q_2/T^2 where Q_1 and Q_2 are positive. As a result the strength of the interplane PD interaction has the form

$$Q = Q_0 - \frac{Q_1}{T} + \frac{Q_2}{T^2} = Q_0 \left(1 - \frac{T_1}{T}\right)\left(1 - \frac{T_2}{T}\right), \quad (110)$$

where $T_1 \simeq 80$ K and $T_2 \simeq 30$ K are temperatures of the spin reorientation transitions. Hence, if $Q_0 > 0$ the magnetic structure is of the first type (La_2NiO_2) if $T > T_1$ and $T < T_2$ and is of the second type (La_2CuO_4) for $T_1 > T > T_2$ [see text after Eq. (41)].

In the end of Sec. VIII we have pointed out the problem of the infrared divergence of the longitudinal spin fluctuations in antiferromagnets. Cuprates and, in particular, Pr_2CuO_4, are very convenient candidates for experimental investigation of these fluctuations. Indeed, there are rather small gaps comparing to the very strong intraplane exchange that is responsible for the quasi-2D infrared divergence[37] that should manifest itself at ω just above $2\Delta_{in}$ where the spin-wave contribution becomes negligible. Corresponding experimental studies would be highly desirable.

In conclusion we present a theoretical description of the spin configuration and spin-wave spectrum of the noncollinear tetragonal AF R_2CuO_4 assuming the PD interaction in CuO_2 planes as well as between them. The inelastic neutron scattering data for Pr_2CuO_4 are presented. They confirm the existence of the PD interaction in this compound and allow us to determine the main parameters of the theory. Comparison of the data for Pr_2CuO_4 and Nd_2CuO_4 (Ref. 14) as well as the undoped AF YBCO (Ref. 36) with the theoretical results of Refs. 22 and 23 reveals a strong dependence of the anisotropic interactions between Cu^{2+} spins on the type of RE ion. The spin configuration of the noncollinear R_2CuO_4 antiferromagnets in canted magnetic field is analyzed as well.

ACKNOWLEDGMENTS

One of the authors (S.M.) is grateful for the financial support of the Russian Foundation for Basic Research (Grant No. 96.02 18037-& 96-15-96775) and the Russian State Programs for Statistical Physics (Grant No. VIII-2). The authors (S.M. and A.I.) thank also the Russian Program ''Neutron Studies of the Condensed Matter.''

APPENDIX A: GROUND-STATE ENERGY IN MAGNETIC FIELD

Here we derive Eq. (85) for the ground-state energy of the system in magnetic field applied in parallel CuO_2 planes. We begin with the collinear case. Then we consider two noncollinear subsystems with the PD interaction between them.

External field rotates neighboring spins in I and II sublattices as shown in Fig. 15. As a result the spin operators may be represented as follows:

$$\vec{S}_\rho = \hat{e}_{\rho z} S_{\rho z} + \hat{e}_{\rho y} S_{\rho y} + \hat{c} S_{\rho x}, \tag{A1}$$

where $\rho = I, II$, $S_{\rho i}$ are given by Eqs. (12) and unit vectors $\hat{e}_{\rho,z(y)}$ have the form [cf. Eq. (11)]

$$\begin{aligned} \hat{e}_{zI} &= [\cos(\varphi+\vartheta), \sin(\varphi+\vartheta), 0], \\ \hat{e}_{zII} &= [-\cos(\varphi-\vartheta), -\sin(\varphi-\vartheta), 0], \\ \hat{e}_{yI} &= [-\sin(\varphi+\vartheta), \cos(\varphi+\vartheta), 0], \\ \hat{e}_{yII} &= [\sin(\varphi-\vartheta), -\cos(\varphi-\vartheta), 0]. \end{aligned} \tag{A2}$$

Substituting these expressions in Eqs. (13),(14),(16) and the Zeeman term of Eq. (3) we obtain in the Hamiltonian consisting from three terms

$$H = E_0 + H_1 + H_2, \tag{A3}$$

where

$$E_0 = NS^2 J_0 [-\tfrac{1}{2} + (\vartheta+\vartheta_0)^2 - \vartheta_0^2] \tag{A4}$$

$$H_1 = \frac{1}{i}\sqrt{\frac{SN}{2}} [g\mu H_\parallel \vartheta (a_0^+ - a_0) - (g\mu H_\perp + 2SJ_0\vartheta)(a_{\mathbf{k}_0}^+ - a_{\mathbf{k}_0})] \tag{A5}$$

$$H_2 = \sum_{\mathbf{k}} [\xi_{\mathbf{k}} a_k^+ a_k + \tfrac{1}{2}(\beta_{\mathbf{k}} a_{\mathbf{k}}^+ a_{-\mathbf{k}}^+ + \beta_k^+ a_{\mathbf{k}} a_{-\mathbf{k}}) - g\mu H_\parallel a_{\mathbf{k}+\mathbf{k}_0}^+ a_{\mathbf{k}}], \tag{A6}$$

where $H_\parallel = H\cos(\psi-\varphi)$ and $H_\perp = H\sin(\psi-\varphi)$ are components of the field parallel and perpendicular to the staggered magnetization, $\vartheta_0 = g\mu H/(2SJ_0)$, $\vartheta \ll 1$. The linear term H_1 appears as a result of the interaction between the canted field with y components of the sublattice magnetization. Here we retain the linear in a and a^+ terms only. Cubic terms should be important at $T > \Delta_0$ (see the end of Sec. VII) as well as at the very vicinity of the spin-flop transition (see below). In Eq. (A6), we should take into account the spin rotation determined by Eq. (A2) and instead of Eqs. (47) we have

$$\begin{aligned} \xi_{\mathbf{k}} &= S[J_0(1-2\vartheta^2) + J_{\mathbf{k}}\vartheta^2 - \tfrac{1}{2}A_{\mathbf{k}} + \tfrac{1}{2}\gamma_{\mathbf{k}}\cos 2\varphi] - g\mu H_\perp \vartheta + \Sigma_{\mathbf{k}}, \\ \beta_{\mathbf{k}} &= S[J_{\mathbf{k}}(1-\vartheta^2) - \tfrac{1}{2}A_{\mathbf{k}} - \tfrac{1}{2}\gamma_{\mathbf{k}}\cos 2\varphi] + \Pi_{\mathbf{k}}, \\ \beta_{\mathbf{k}}^+ &= S[J_{\mathbf{k}}(1-\vartheta^2) - \tfrac{1}{2}A_{\mathbf{k}} - \tfrac{1}{2}\gamma_{\mathbf{k}}\cos 2\varphi] + \Pi_{\mathbf{k}}^+, \end{aligned} \tag{A7}$$

where $J_{\mathbf{k}}$, $A_{\mathbf{k}}$, $\gamma_{\mathbf{k}}$, $\Sigma_{\mathbf{k}}$, $\Pi_{\mathbf{k}}$, and $\Pi_{\mathbf{k}}^+$ are given by Eqs. (18), (24), (50), and (57). Hence, Eq. (A6) may be considered as an effective non-Hermitian Hamiltonian.

The interaction H_1 is linear in operators a and a^+. It should be eliminated using the substitution

$$\begin{aligned} a_p &\to a_p - i\left(\frac{NS}{2}\right)^{1/2}\mu_p, \\ a_p^+ &\to a_p^+ + i\left(\frac{NS}{2}\right)^{1/2}\mu_p^+, \end{aligned} \tag{A8}$$

where $p = 0, \mathbf{k}_0$; μ_p and μ_p^+ are c numbers. Similar substitution appears in the theoretical consideration of the diluted Bose gas below T_c and is a result of the Bose condensation.[30,33] The linear term in the Hamiltonian disappears if μ_p and μ_p^+ satisfy the following equations:

$$\begin{aligned} \xi_0\mu_0 - \beta_0\mu_0^+ - K\mu_{\mathbf{k}_0} &= -K\vartheta, \\ -\beta_0^+\mu_0 + \xi_0\mu_0^+ - K\mu_{\mathbf{k}_0}^+ &= -K\vartheta, \\ -K\mu_0 + \xi_{\mathbf{k}_0}\mu_{\mathbf{k}_0} - \beta_{\mathbf{k}_0}\mu_{\mathbf{k}_0}^+ &= \Lambda, \\ -K\mu_0^+ - \beta_{\mathbf{k}_0}^+\mu_{\mathbf{k}_0} + \xi_{\mathbf{k}_0}\mu_{\mathbf{k}_0}^+ &= \Lambda, \end{aligned} \tag{A9}$$

where $K = g\mu H_\parallel$ and $\Lambda = g\mu H_\perp \vartheta + 2SJ_0$. The solution of this system is given by

$$\begin{aligned} \mu_0 = -\{&K\vartheta[(\xi_0+\beta_0)(\xi_{\mathbf{k}_0}^2 - \beta_{\mathbf{k}_0}\beta_{\mathbf{k}_0}^+) - (\xi_{\mathbf{k}_0} - \beta_{\mathbf{k}_0})K^2] \\ &+ K\Lambda[\xi_0(\xi_{\mathbf{k}_0}+\beta_{\mathbf{k}_0}) + \beta_{\mathbf{k}_0}(\xi_{\mathbf{k}_0}+\beta_{\mathbf{k}_0}^+) - K^2]\} d_0^{-1}, \\ \mu_{\mathbf{k}_0} = \{&-K^2\vartheta[(\xi_0\xi_{\mathbf{k}_0} + \xi_0\beta_{\mathbf{k}_0} + \xi_{\mathbf{k}_0}\beta_0 + \beta_{\mathbf{k}_0}\beta_0^+) - K^2] \\ &+ \Lambda[(\xi_{\mathbf{k}_0}+\beta_{\mathbf{k}_0})(\xi_0^2 - \beta_0\beta_0^+) + (\beta_0 - \xi_0)K^2]\} d_0^{-1}, \end{aligned} \tag{A10}$$

where

$$d_0 = (\xi_0^2 - \beta_0\beta_0^+)(\xi_{\mathbf{k}_0}^2 - \beta_{\mathbf{k}_0}\beta_{\mathbf{k}_0}^+) - K^2(2\xi_0\xi_{\mathbf{k}_0} + \beta_0\beta_{\mathbf{k}_0}^+ + \beta_0^+\beta_{\mathbf{k}_0}) + K^4 \tag{A11}$$

and expressions for μ_0^+ and $\mu_{\mathbf{k}_0}^+$ follow from Eqs. (A10) after replacement $\beta \to \beta^+$ and $\beta^+ \to \beta$. At the same time, from Eq. (A8) we have

$$\mu_p^+ = \mu_p^*. \tag{A12}$$

According to Eqs. (49) and (A7) in our approximation we have

$$\xi_0^2-\beta_0\beta_0^+=2SJ_0(2\xi_0-\beta_0-\beta_0^+)=\Delta_{in}^2(\varphi,H),$$
$$\xi_{\mathbf{k_0}}^2-\beta_{\mathbf{k_0}}\beta_{\mathbf{k_0}}^+=2SJ_0(2\xi_{\mathbf{k_0}}+\beta_{\mathbf{k_0}}+\beta_{\mathbf{k_0}}^+)=\Delta_{R\,out}^2, \quad \text{(A13)}$$

where

$$\Delta_{in}^2(\varphi,H)=\Delta_0^2\cos 4\varphi-(2SJ_0\vartheta)(g\mu H_\perp). \quad \text{(A14)}$$

Using these expressions and Eq. (50) we get

$$d_0=(\Delta_{R\,out}^2-K^2)[\Delta_{in}^2(\varphi,H)-K^2], \quad \text{(A15)}$$

$$\mu_0=\mu_0^+=(g\mu H_\parallel g\mu H_\perp)[\Delta_{in}^2(\varphi,H)-K^2]^{-1}. \quad \text{(A16)}$$

At the same time we obtain

$$\mu_{\mathbf{k_0}}=d_0^{-1}\Big\{-K^2\vartheta(\Delta_{R\,out}^2-K^2)+\Lambda\Big[\Delta_{in}^2(\Delta_{R\,out}^2-K^2)\times(2SJ_0)^{-1}-(\Delta_{in}^2-K^2)2J_0N^{-1}\sum_{\mathbf{k}}n_{\mathbf{k}}\Big]\Big\} \quad \text{(A17)}$$

and the expression for $\mu_{\mathbf{k_0}}^+$ that differs by sign in front of the last term in the square brackets. Hence, the condition (A12) may be fulfilled only if $\Lambda=0$ and we have

$$\vartheta=-\vartheta_0=-\frac{g\mu H_\perp}{2SJ_0}. \quad \text{(A18)}$$

Using this expression and Eqs. (A10), (A13)–(A15) we get

$$\mu_0=\mu_0^+=\frac{g\mu H_\parallel g\mu H_\perp}{\Delta_0^2\cos 4\varphi+(g\mu H_\perp)^2-(g\mu H_\parallel)^2},$$
$$\mu_{\mathbf{k_0}}=\mu_{\mathbf{k_0}}^+=\frac{g\mu H_\parallel}{2SJ_0}\mu_0. \quad \text{(A19)}$$

Substitution (A8) gives rise to a contribution to the ground-state energy that may be represented in the following general form:

$$\Delta E=\tfrac{1}{2}\mu_iC_{ik}\mu_k+D_i\mu_i.$$

It is easy to show that Eqs. (A9) coincide with the conditions

$$\frac{\partial\Delta E}{\partial\mu_i}=C_{ik}\mu_k+D_i=0. \quad \text{(A20)}$$

As a result we have from Eqs. (A5)

$$\Delta E=\frac{D_i\mu_i}{2}=-\frac{SNg\mu H_\parallel\vartheta_0\mu_0}{2} \quad \text{(A21)}$$

and using Eqs. (39), (A4), and (A19) for the ground-state energy we obtain Eq. (87) in Sec. VII.

These results are based on the linear approximation $S_{y0}=i(S/2)^{1/2}(a_0^+-a_0)$ and are valid if $\mu_0\ll 1$. Meanwhile for the field along the [1,1,0] direction close to the spin-flop transition when $r=(g\mu H/\Delta_0)\to 1$ we have $\mu=r^2/[2(1-r^4)^{1/2}]$ and $\mu=r^2/[6(1-r)^{1/4}]$ for the rotation angle φ determined by Eqs. (89) and (92), respectively, and the linear approximation fails. In this case the nonlinear term in the expression for S_{y0} becomes important. This term follows from Eqs. (12) and after substitution (A8) S_{y0} acquires a factor $f=(1-\mu^2/8)$, which becomes important very close to the transition only. Indeed, setting for example, $r=0.9$ we get $f=0.94$ and $f=0.993$ for the two cases mentioned above, respectively. Moreover, in the second case where $\alpha=\varphi+\pi/4$ is given by Eq. (92) if $r=0.99$ we get $\mu=0.52$ and $f=0.97$. Hence, we may use the linear approximation near the transition too except for a very narrow region where the critical fluctuations become important. However, consideration of this problem is beyond the scope of our paper.

For the noncollinear spin structure one has to take into account the interaction between two subsystems given by Eqs. (22) and (25). As above the magnetic field gives rise to linear terms in the Hamiltonian in the form given by Eq. (A5) that acquire an additional index $i=1,2$ labeling the subsystems. The interaction W_1 given by Eq. (21) should be taken into account too. These linear terms should be eliminated by the substitution (A8) where now p is equal to 0,i and $\mathbf{k}_0,i$, respectively, and $i=1,2$. As a result instead of four Eqs. (A9) we get

$$\tilde{\xi}_{01}\mu_{01}-\beta_{01}\mu_{01}^+-K_1\mu_{\mathbf{k}_0 1}+C_0\mu_{20}-D_0\mu_{20}^+=X_1,$$
$$-\beta_{01}^+\mu_{01}+\tilde{\xi}_{01}\mu_{01}^+-K_1\mu_{\mathbf{k}_0 1}^+-D_0\mu_{20}+C_0\mu_{20}^+=X_1,$$
$$-K_1\mu_{01}+\tilde{\xi}_{\mathbf{k}_0 1}\mu_{\mathbf{k}_0 1}-\beta_{\mathbf{k}_0 1}\mu_{\mathbf{k}_0 1}^+ +C_{\mathbf{k}_0}\mu_{2\mathbf{k}_0}-D_{\mathbf{k}_0}\mu_{2\mathbf{k}_0}^+=\Lambda_1,$$
$$-K_1\mu_{01}^+-\beta_{\mathbf{k}_0 1}^+\mu_{\mathbf{k}_0 1}+\tilde{\xi}_{\mathbf{k}_0 1}\mu_{\mathbf{k}_0 1}^+-D_{\mathbf{k}_0}\mu_{2\mathbf{k}_0}+C_{\mathbf{k}_0}\mu_{2\mathbf{k}_0}^+=\Lambda_1, \quad \text{(A22)}$$

and another four equations which follow from Eq. (A22) by replacement $(1\rightleftharpoons 2)$. Here

$$\tilde{\xi}_{\mathbf{k}1,2}=\xi_{\mathbf{k}1,2}+R_0,\quad R_0=-SQ_{\mathbf{k}_0}^{ab}\sin(\varphi_1+\varphi_2);$$
$$K_{1,2}=g\mu H_{\parallel,1,2},\quad \Lambda_{1,2}=g\mu H_{\perp,1,2}+2SJ_0\vartheta_{1,2};$$
$$C_0=\tfrac{1}{2}(SM_0+R_0),\quad D_0=\tfrac{1}{2}(SM_0-R_0); \quad \text{(A23)}$$
$$X_{1,2}=-g\mu H_{\perp 1,2}\vartheta_{1,2}+SQ_{\mathbf{k}_0}\cos(\varphi_1+\varphi_2);$$
$$C_{\mathbf{k}_0}=-D_{\mathbf{k}_0}=\frac{S}{2}M_0\cos(\varphi_1-\varphi_2).$$

It may be shown that as above from the conditions (A12) one obtains $\Lambda_{1,2}=0$ and we get

$$\vartheta_{1,2}=-\vartheta_{01,2}=-\frac{g\mu H_{\perp 1,2}}{2SJ_0}. \quad \text{(A24)}$$

This point will be discussed below.

For the solution of eight equations for μ_p and μ_p^+ we define a vector

$$\mu_0=(\mu_1,\mu_1^+,\mu_2,\mu_2^+,\overline{\mu_1},\overline{\mu_1^+},\overline{\mu_2},\overline{\mu_2^+})=(\mu,\overline{\mu}), \quad \text{(A25)}$$

where $\mu_1=\mu_{01}$, $\overline{\mu_1}=\mu_{\mathbf{k}_0 1}$, etc. Here and below the bar denotes states with $\mathbf{k}+\mathbf{k}_0$. In Eqs. (A22) the K terms mix μ and $\overline{\mu}$ and we may write

$$\left[\begin{pmatrix} Z, & 0 \\ 0, & \overline{Z} \end{pmatrix} - \begin{pmatrix} 0, & K \\ K, & 0 \end{pmatrix}\right]\begin{pmatrix} \mu \\ \overline{\mu} \end{pmatrix} = \begin{pmatrix} U \\ \overline{U} \end{pmatrix}, \tag{A26}$$

where

$$Z = \begin{pmatrix} \tilde{\xi}_1, -\beta_1, C_0, -D_0 \\ -\beta_1^+, \tilde{\xi}_1, -D_0, C_0 \\ C_0, -D_0, \tilde{\xi}_2, -\beta_2 \\ -D_0, C_0, -\beta_2^+, \tilde{\xi}_2 \end{pmatrix}, \quad \overline{Z} = \begin{pmatrix} \tilde{\bar{\xi}}_1, -\overline{\beta}_1, \overline{C}, \overline{C} \\ -\overline{\beta}_1^+, \overline{\xi}_1, \overline{C}, \overline{C} \\ \overline{C}, \overline{C}, \tilde{\bar{\xi}}_2, -\overline{\beta}_2 \\ \overline{C}, \overline{C}, -\overline{\beta}_2, \tilde{\bar{\xi}}_2 \end{pmatrix};$$

$$K = \begin{pmatrix} \tilde{K}_1, & 0 \\ 0, & \tilde{K}_2 \end{pmatrix}, \quad \tilde{K}_{1,2} = \begin{pmatrix} K_{1,2} & 0 \\ 0 & K_{1,2} \end{pmatrix}; \tag{A27}$$

$$U = (X_1, X_1, X_2, X_2)$$

and from Eq. (A24) it follows that $\overline{U}=0$. As a result we obtain

$$\begin{gathered} (Z - K\overline{Z}^{-1}K)\mu = U, \\ \overline{\mu} = \overline{Z}^{-1}K\mu. \end{gathered} \tag{A28}$$

Using the above-mentioned approximation we have

$$\overline{Z}^{-1} = \begin{pmatrix} \overline{Z}_1^{-1} & 0 \\ 0 & \overline{Z}_2^{-1} \end{pmatrix}, \quad Z_{1,2}^{-1} = \frac{1}{\overline{\epsilon^2}}\begin{pmatrix} \tilde{\bar{\xi}}_{1,2}, & -\overline{\beta}_{1,2} \\ -\overline{\beta}_{1,2}^+, & \tilde{\bar{\xi}}_{1,2} \end{pmatrix}, \tag{A29}$$

where $\overline{\epsilon^2} = \Delta_{out}^2$ and Δ_{out}^2 is given by Eq. (61). By these expressions we reduce our problem to the solution of four linear equations that may be easily done and we get

$$\begin{aligned} \mu_{0,1} = \{ & X_1[(E_1+B_1)(E_2^2 - B_2B_2^+) - (C_0+D_0)^2E_2 \\ & + (C_0+D_0)(C_0B_2 + D_0B_2^+)] \\ & + X_2[D_0(E_1E_2 + E_1B_2^+ + E_2B_1 + B_1B_2) \\ & - C_0(B_1E_2 + B_1B_2^+ + E_1B_2 + E_1E_2) \\ & + (C_0 - D_0)(C_0^2 - D_0^2)]\}d^{-1}, \end{aligned} \tag{A30}$$

where $E_{1,2} = \tilde{\xi}_{01,2} - K_{1,2}^2\tilde{\bar{\xi}}_{1,2}/\overline{\epsilon^2}$, $B_{1,2} = \beta_{01,2} + K_{1,2}^2\overline{\beta}_{1,2}/\overline{\epsilon^2}$ and similar expression for $B_{1,2}^+$. The determinant d is given by

$$\begin{aligned} d = & (E_1^2 - B_1B_1^+)(E_2^2 - B_2B_2^+) - (C_0 - D_0)^2 \\ & - C_0^2(2E_1E_2 + B_1B_2^+ + B_1^+B_2) \\ & - D_0^2(2E_1E_2 + B_1B_2 + B_1^+B_2^+) \\ & + 2C_0D_0[E_1(B_2 + B_2^+) + E_2(B_1 + B_1^+)]. \end{aligned} \tag{A31}$$

The expression for $\mu_{0,1}^+$ follows from Eq. (A30) if one replaces $B_{1,2}$ with $B_{1,2}^+$ and vice versa.

As pointed in Sec. III the interaction between subsystems is very weak and C and D terms should be retained if they are multiplied by the large factor SJ_0 only. As a result, from Eqs. (A30),(A31) we obtain final expressions in the form

$$\begin{aligned} \mu_{0,1} = \mu_{0,1}^+ = 2SJ_0\{ & X_1[\Delta_{in,2}^2 + 2SJ_0R_0 - (g\mu H_{\|,2})^2] \\ & - 2SJ_0R_0X_2\}\{[\Delta_{in,1}^2 + 2SJ_0R_0 - (g\mu H_{\|,1})^2] \\ & \times [\Delta_{in,2}^2 + 2SJ_0R_0 - (g\mu H_{\|,2})^2] - (2SJ_0R_0)^2\}^{-1}, \end{aligned} \tag{A32}$$

where $\Delta_{in,1,2}^2$ are determined by Eqs. (A14),(A24) and similar expression for $\mu_{0,2} = \mu_{0,2}^+$.

In the same way as above using Eqs. (A5),(A8) and conditions $\Lambda_{1,2}=0$ we get

$$\Delta E = -\frac{NS}{2}(X_1\overline{\mu}_{0,1} + X_2\overline{\mu}_{0,2})(2SJ_0)^{-1} \tag{A33}$$

and Eq. (85) in Sec. VII immediately follows from Eqs. (A32) and (A33).

We justify now Eqs. (A24). In our approximation parts of μ and μ^+ that depend on the interaction between subsystems are independent on the small difference between β and β^+. Meanwhile, μ and μ^+ have terms proportional to $\Lambda_{1,2}$ as in Eq. (A17) and condition (A12) may be fulfilled if $\Lambda_{1,2}=0$ only.

It should be noted that Eqs. (A32) and (A33) as well as the expression (85) for the ground-state energy are valid for $\mu_{01,2} \ll 1$ only. If $\mu_{01,2} \gtrsim 1$ one has to extract condensate contribution from the interaction energy (44) as in the case of the Bose gas[30,32] and lower-order terms. Then the condensate amplitudes $\mu_{01,2}$ should be determined self-consistently. The second-order terms give rise to an additional contribution to the parameters $\xi_{1,2}$, $\beta_{1,2}$, and $\beta_{1,2}^+$ of the effective Hamiltonian and the gaps acquire corrections proportional to $\mu_{01,2}^2$. However, detailed investigation of this problem is beyond the scope of this paper. We comment only on two cases considered in the main text: (i) $\mathbf{H} \| [1,1,0]$ and (ii) $\mathbf{H} \| \hat{a}$. In the former case we have $\cos(\varphi_1 + \varphi_2) = 0$ and the problem is the same as for two noninteracting systems of planes (see above and Sec. VII). For $\mathbf{H}$ along the $\hat{a}$ axis below the spin-flop transition we have $\mu_{01,2}=0$. However, in the flopped state $\cos(\varphi_1+\varphi_2) = \pm 1$ and

$$\mu_{01,2} = \pm 2SJ_0Q_{\mathbf{k}_0}[\Delta_0^2 + (g\mu H)^2]^{-1}. \tag{A34}$$

Taken into account Eq. (93) for the flop field we obtain $|\mu_{01,2}| \gg 1$ near the transition, and the theory should be revised as it stated above. In particular, Δ_0 in Eq. (102) does not have to coincide with the in-plane gap at $\mathbf{H}=0$.

APPENDIX B: GREEN'S FUNCTIONS IN MAGNETIC FIELD

Here we evaluate expressions for the Green's functions in magnetic field using the non-Hermitian Hamiltonian (A6), which takes into account the interaction between spin waves. From Eqs. (27), (A5), and (A6) we get

$$
\begin{aligned}
&(\omega-\tilde{\xi}_1)G_{11}-\beta_1 F_{11}^{+}-CG_{21}-DF_{21}^{+}+K_1\overline{G}_{11}=1,\\
&\beta_1^{+}G_{11}+(\omega+\tilde{\xi}_1)F_{11}^{+}+DG_{21}+CF_{21}^{+}-K_1\overline{F}_{11}^{+}=0,\\
&-CG_{11}-DF_{11}^{+}+(\omega-\tilde{\xi}_2)G_{21}-\beta_2 F_{21}^{+}+K_2\overline{G}_{21}=0,\\
&DG_{11}+CF_{11}^{+}+\beta_2^{+}G_{21}+(\omega+\tilde{\xi}_2)F_{21}^{+}-K_2\overline{F}_{21}^{+}=0,\\
&K_1G_{11}+(\omega-\bar{\tilde{\xi}}_1)\overline{G}_{11}-\overline{\beta}_1\overline{F}_{11}^{+}-\overline{CG}_{21}-\overline{DF}_{21}^{+}=0,\\
&-K_1F_{11}^{+}+\overline{\beta}_1^{+}\overline{G}_{11}+(\omega+\bar{\tilde{\xi}}_1)\overline{F}_{11}^{+}+\overline{DG}_{21}+\overline{CF}_{21}^{+}=0,\\
&K_2G_{21}-\overline{CG}_{11}-\overline{DF}_{11}^{+}+(\omega-\bar{\tilde{\xi}}_2)\overline{G}_{21}-\overline{\beta}_2\overline{F}_{21}^{+}=0,\\
&-K_2\overline{F}_{21}^{+}+\overline{DG}_{11}+\overline{CF}_{11}^{+}+\overline{\beta}_2^{+}\overline{G}_{21}+(\omega+\bar{\tilde{\xi}}_2)\overline{F}_{21}^{+}=0,
\end{aligned}
\tag{B1}
$$

where as above 1 and 2 label the subsystems and the bar denotes substitution of one $\mathbf{k}$ by $\mathbf{k}+\mathbf{k}_0$. For example, $\bar{\tilde{\xi}}_1=\tilde{\xi}_{1,\mathbf{k}+\mathbf{k}_0}$ and $\overline{G}_{21}=G_{21\,\mathbf{k}+\mathbf{k}_0,\mathbf{k}}$.

Due to the non-Hermiticity of the Hamiltonian (A6) for calculation of final physical results we need also the solution of the system conjugated to Eqs. (B1). Corresponding Green's functions may be obtained from the solution of Eq. (B1) by the replacement $\omega\to-\omega$, $\beta\to\beta^{+}$, and $\beta^{+}\to\beta$.

Equations (B1) may be solved in the same way as (A22) if one takes into account that only K terms in the left-hand side mix functions with and without the bar. As a result Eqs. (B1) may be rewritten as follows:

$$
\begin{pmatrix} m, & K \\ K, & \overline{m} \end{pmatrix}\begin{pmatrix} g_{11}, g_{12} \\ g_{21}, g_{22} \end{pmatrix}=\begin{pmatrix} I, & 0 \\ 0, & 0 \end{pmatrix},
\tag{B2}
$$

where

$$
m=\begin{pmatrix} m_1, & L \\ L, & m_2 \end{pmatrix};\quad K=\begin{pmatrix} \tilde{K}_1, & 0 \\ 0, & \tilde{K}_2 \end{pmatrix};\quad I=\begin{pmatrix} I_0, & 0 \\ 0, & 0 \end{pmatrix}
\tag{B3}
$$

and

$$
\begin{aligned}
m_{1,2}&=\begin{pmatrix} \omega-\tilde{\xi}_{1,2}, & -\beta_{1,2} \\ \beta_{1,2}^{+} & \omega+\tilde{\xi}_{1,2} \end{pmatrix};\quad L=\begin{pmatrix} -C, & -D \\ D, & C \end{pmatrix};\\
\tilde{K}_{1,2}&=\begin{pmatrix} K_{1,2}, & 0 \\ 0 & -K_{1,2} \end{pmatrix};\quad I_0=\begin{pmatrix} 1, & 0 \\ 0, & 0 \end{pmatrix}.
\end{aligned}
\tag{B4}
$$

From Eq. (B2) we get

$$
(m-K\overline{m}^{-1}K)g_{11}=I.
\tag{B5}
$$

The corresponding equation for $\overline{g}_{11}$ has the form

$$
(\overline{m}-Km^{-1}K)\overline{g}_{11}=I.
\tag{B6}
$$

Taking now into account that $g\mu H\ll SJ_0$ we have to calculate matrix elements of $(\overline{m}^{-1})_{ik}$ and $(m^{-1})_{ik}$, neglecting in numerators terms that are proportional to interplane coupling $\overline{C}(C)$ and $\overline{D}(D)$. As a result we get

$$
\overline{m}^{-1}=\begin{pmatrix} \overline{m}_1^{-1}, & 0 \\ 0, & \overline{m}_2^{-1} \end{pmatrix},
\tag{B7}
$$

where

$$
\overline{m}_{1,2}^{-1}=\frac{1}{\omega^2-\overline{\epsilon^2}}\begin{pmatrix} \omega+\bar{\tilde{\xi}}_{1,2}, & \overline{\beta}_{1,2} \\ -\overline{\beta}_{1,2}^{+}, & \omega-\bar{\tilde{\xi}}_{1,2} \end{pmatrix}
\tag{B8}
$$

and $\overline{\epsilon^2}=\overline{\epsilon}_{1,2}^2=\Delta_{R\,out}^2+S^2(J_0-J_{\mathbf{k}}^2)$ where $\Delta_{R\,out}^2$ is given by Eq. (61). As a result we obtain the following equation:

$$
\begin{pmatrix} m_1-\tilde{K}_1\overline{m}_1^{-1}\tilde{K}_1, & L \\ L, & m_2-\tilde{K}_2\overline{m}_2^{-1}\tilde{K}_2 \end{pmatrix}g_{11}=I.
\tag{B9}
$$

This system of four equations may be solved directly and in the approximation used above [see text before Eq. (A32)] we have

$$
\begin{aligned}
G_{11}&=\frac{d_2}{Z}[(\omega+\xi_1)(\omega^2-\overline{\epsilon^2})-K_1^2(\omega-\overline{\xi_1})],\\
F_{11}^{+}&=-\frac{d_2}{Z}[\beta_1^{+}(\omega^2-\overline{\epsilon^2})-K_1^2\overline{\beta}_1^{+}],
\end{aligned}
\tag{B10}
$$

$$
G_{21}=-F_{21}^{+}=\frac{2}{Z}(\omega^2-\overline{\epsilon^2}+K_1^2)(\omega^2-\overline{\epsilon^2}+K_2^2)(SJ_0)^2(C-D),
$$

where we set $J_{\mathbf{k}}=J_0$ where

$$
d_2(\omega)=(\omega^2-\epsilon_2^2)(\omega^2-\overline{\epsilon^2})-K_2^2(2\omega^2+\epsilon_2^2+\overline{\epsilon^2})+K_2^4
\tag{B11}
$$

is the determinant of the matrix $m_2-\tilde{K}_2\overline{m}_2^{-1}\tilde{K}_2$ multiplied by $(\omega^2-\overline{\epsilon^2})$, $\epsilon_{1,2}^2=\tilde{\xi}_{1,2}^2-\beta_{1,2}\beta_{1,2}^{+}$ and

$$
\begin{aligned}
Z(\omega)&=d_1(\omega)d_2(\omega)-[2SJ_0(C-D)]^2\\
&\quad\times(\omega^2-\overline{\epsilon^2}+K_1^2)(\omega^2-\overline{\epsilon^2}+K_2^2).
\end{aligned}
\tag{B12}
$$

Obviously the equation $Z(\omega)=0$ determines the spin-wave spectrum along the $\hat{c}$ direction at $H\neq0$, which has now four branches. However, taking into account that in real systems $\Delta_{out}^2\gg K_{1,2}^2,\epsilon_{1,2}^2$ we may strongly simplify these expressions. Neglecting small splitting of two modes with $\omega\simeq\Delta_{out}^2$ we obtain

$$
\begin{aligned}
G_{11}&\simeq-F_{11}^{+}\simeq\frac{SJ_0(\omega^2-\epsilon_2^2+K_2^2)}{(\omega^2-\epsilon_{+}^2)(\omega^2-\epsilon_{-}^2)},\\
G_{21}&\simeq-F_{21}^{+}\simeq\frac{2(SJ_0)^2(C-D)}{(\omega^2-\epsilon_{+}^2)(\omega^2-\epsilon_{-}^2)},
\end{aligned}
\tag{B13}
$$

where

$$
\begin{aligned}
\epsilon_{\pm}^2&=\tfrac{1}{2}\{\epsilon_1^2+\epsilon_2^2-K_1^2-K_2^2\\
&\quad\pm[(\epsilon_1^2-\epsilon_2^2-K_1^2+K_2^2)^2+16(SJ_0)^2(C-D)^2]^{1/2}\}.
\end{aligned}
\tag{B14}
$$

In particular, for the field along the [1,1,0] direction ϵ_+ and ϵ_- coincide with optical and acoustic branches given by Eqs. (60) with Δ_0^2 replaced by $\Delta_0^2\cos 4\varphi$. We must remind that these results are valid for $k_{a,b} \ll \pi/a$ only.

We need also the functions $\overline{G}$ and $\overline{F}$ which are solutions of Eq. (B6). In this case we have

$$m^{-1}=\frac{d_1 d_2}{d}\begin{pmatrix} m_1^{-1} & 0 \\ 0 & \overline{m_2}^{-1} \end{pmatrix}, \tag{B15}$$

where $d_{1,2}=\omega^2-\epsilon_{1,2}^2$ and

$$d=d_1 d_2-[2SJ_0(C-D)]^2 \tag{B16}$$

and Eq. (B6) may be represented as follows:

$$\begin{pmatrix} \overline{m}_1-\frac{d_1 d_2}{d}\tilde{K}_1 m_1^{-1}\tilde{K}_1, & \overline{L} \\ \overline{L}, & \overline{m}_2-\frac{d_1 d_2}{d}\tilde{K}_2 m_2^{-1}\tilde{K}_2 \end{pmatrix}\overline{g}_{11}=I. \tag{B17}$$

Solution of this equation is given by

$$\overline{G}_{11}=\overline{F}_{11}^{+}=\frac{SJ_0}{Z_1}(d+d_1K_1^2),$$
$$\overline{G}_{21}=\overline{F}_{21}^{+}=0, \tag{B18}$$

where

$$Z_{1,2}=(\omega^2-\Delta_{out}^2)d-\Delta_{out}^2K_{1,2}^2 d_{1,2}. \tag{B19}$$

Using the same approximations as above we obtain the final expression in the form

$$\overline{G}_{11}=\overline{F}_{11}^{+}=\frac{SJ_0}{\omega^2-\Delta_{out}^2}, \tag{B20}$$

which holds for $\mathbf{k}=(\mathbf{k}_0,k_c)$.

The spin-wave spectrum in magnetic field is determined by the condition $Z(\omega)=0$ where $Z(\omega)$ is given by Eq. (B12) and $Z(0)$ is a product of squared spin-wave frequencies and should be positive. For this value we have

$$Z(0)=(\overline{\epsilon^2}-K_1^2)(\overline{\epsilon^2}-K_2^2)$$
$$\times[(\epsilon_1^2-K_1^2)(\epsilon_2^2-K_2^2)-(2SJ_0R_{\mathbf{k}})^2]. \tag{B21}$$

Here at $\mathbf{k}=0$ the expression in the square brackets coincides with the denominator of the second term in Eq. (85). Experimentally the out-of-plane gap is much larger than the in-plane one and we conclude that the positiveness of the square brackets is the necessary condition of the stability of the system, which has been used in derivation of Eq. (93).

[1] I.W. Sumarlin, J.W. Lynn, T. Chattopadhyay, S.N. Barilo, D.I. Zhigunov, and J.L. Peng, Phys. Rev. B **51**, 5824 (1995).

[2] D. Petitgrand, A.H. Moudden, P. Galez, and P. Boutrouille, J. Less-Common Met. **164-165**, 768 (1990).

[3] S. Skanthakumar, J.W. Lynn, J.L. Peng, and Z.Y. Li, Phys. Rev. B **47**, 6173 (1993).

[4] S. Skanthakumar, J.W. Lynn, J.L. Peng, and Z.Y. Li, J. Appl. Phys. **73**, 6326 (1993).

[5] T. Chattopadhyay, J.W. Lynn, N. Rosov, T.E. Grigereit, S.N. Barilo, and D.I. Zhigunov, Phys. Rev. B **49**, 9944 (1994).

[6] D. Vaknin, S.K. Sinha, C. Stassis, L.L. Miller, and D.C. Johnston, Phys. Rev. B **41**, 1926 (1990).

[7] M. Greven, R.J. Birgeneau, Y. Endoh, M.A. Kastner, M. Matsuda, and G. Shirane, Phys. Rev. Lett. **72**, 1096 (1994).

[8] D.A. Yablonsky, Physica C **182**, 105 (1991).

[9] R. Sachidanandam, T. Yildirim, A.B. Harris, A. Aharony, and O. Entin-Wohlman, Phys. Rev. B **56**, 260 (1997).

[10] M. Matsuda, K. Yamada, K. Kakurai, H. Kadowaki, T.R. Thurston, Y. Endoh, Y. Hidaka, R.J. Birgeneau, M.A. Kastner, P.M. Gehring, A.H. Moudden, and G. Shirane, Phys. Rev. B **42**, 10 098 (1990).

[11] P. Vigoureux, A. Gukasov, S.N. Barilo, and D.I. Zhigunov, Physica B **234-236**, 815 (1997).

[12] V.P. Plakhty, A.B. Stratilatov, and S. Beloglazov, Solid State Commun. **103**, 683 (1997).

[13] M. Braden, W. Paulus, A. Cousson, P. Vigoureux, G. Heger, A. Gukasov, Ph. Bourges, D. Petitgrand, Europhys. Lett. **25**, 625 (1994).

[14] A.S. Ivanov, Ph. Bourges, D. Petitgrand, and J. Rossat-Mignod, Physica B **213-214**, 60 (1995).

[15] P. Thalmeier, Physica C **266**, 89 (1996).

[16] W. Henggeler, T. Chattopadhyay, P. Thalmeier, P. Vorderwish, and A. Furrer, Europhys. Lett. **34**, 537 (1996).

[17] H. Casalta, Ph. Bourges, D. Petitgrand, and A.S. Ivanov, Solid State Commun. **100**, 683 (1996).

[18] H. Casalta, Ph. Bourges, M. d'Astuto, D. Petitgrand, and A. Ivanov, Phys. Rev. B **57**, 471 (1998).

[19] Ph. Bourges, L. Boudarene, and D. Petitgrand, Physica B **180-181**, 128 (1992); B. Gillon, D. Petitgrand, P. Galez, J.C. Castaing, and P. Schweiss, J. Magn. Magn. Mater. **104-107**, 583 (1992).

[20] F.C. Chou, A. Aharony, R.J. Birgeneau, O. Entin-Wohlman, M. Greven, A.B. Harris, M.A. Kastner, Y.J. Kim, D.S. Kleinberg, Y.S. Lee, and Q. Zhu, Phys. Rev. Lett. **78**, 535 (1997).

[21] T. Yildirim, A.B. Harris, O. Entin-Wohlman, and A. Aharony, Phys. Rev. Lett. **72**, 3710 (1994).

[22] T. Yildirim, A.B. Harris, A. Aharony, and O. Entin-Wohlman, Phys. Rev. B **52**, 10 239 (1995).

[23] O. Entin-Wohlman, A.B. Harris, and A. Aharony, Phys. Rev. B **53**, 11 661 (1996).

[24] S.V. Maleyev, Pis'ma Zh. Éksp. Teor. Fiz. **61**, 43 (1995) [JETP Lett. **61**, 44 (1995)].

[25] J. Kondo, Prog. Theor. Phys. **27**, 772 (1962).

[26] S.V. Maleyev, Pis'ma Zh. Éksp. Teor. Fiz. **68**, 67 (1998) [JETP Lett. **68**, 71 (1998)].

[27] P.-A. Lindgård, Phys. Rev. Lett. **78**, 4641 (1997).

[28] V.P. Plakhty, S.V. Maleyev, S. Gavrilov, O.P. Smirnov, and P. Burlet, Phys. Lett. A (to be published).

[29] V.G. Vaks, A.I. Larkin, and S.A. Pikin, Zh. Éksp. Teor. Fiz. **53**, 281 (1967) [Sov. Phys. JETP **26**, 188 (1968)].
[30] A.A. Abrikosov, L.P. Gor'kov, and I.E. Dzyaloshinsky, *Quantum Field Theoretical Methods in Statistical Physics* (Pergamon, New York, 1965).
[31] J. Igarashi, Phys. Rev. B **46**, 10 763 (1992).
[32] K. Hida, J. Phys. Soc. Jpn. **59**, 2230 (1990).
[33] S.T. Belyaev, Zh. Éksp. Teor. Fiz. **34**, 417 (1959) [Sov. Phys. JETP **7**, 289 (1958)]; **34**, 433 (1959) [**7**, 299 (1958)].
[34] V.V. Eremenko, S.A. Zvyagin, V.V. Pishko, V.V. Tsapenko, S.N. Barilo, and D.I. Zhigunov, Pis'ma Zh. Éksp. Teor. Fiz. **52**, 955 (1990) [JETP Lett. **52**, 338 (1990)].
[35] Ph. Bourges, H. Casalta, A.S. Ivanov, and D. Petitgrand, Phys. Rev. Lett. **79**, 4906 (1997).
[36] P. Burlet, J.Y. Henry, and L.P. Regnault, Physica C **296**, 205 (1998).
[37] S. Braune and S.V. Maleyev, Z. Phys. B **81**, 69 (1990).
[38] B.P. Toperverg and A.G. Yashenkin, Phys. Rev. B **48**, 16 505 (1993).
[39] J. Villain, R. Bidaux, J.P. Carton, and R. Conte, J. Phys. (Paris) **41**, 1263 (1980).
[40] T. Yildirim, A.B. Harris, and E.F. Shender, Phys. Rev. B **53**, 6455 (1996).
[41] We note that upon decreasing temperature (below ~20 K), an increase of the small in-plane gap has been recently observed in Pt_2CuO_4 [A. S. Ivanov, Ph. Bourges, and D. Petitgrand, *Proceedings of SCES'98 Conference* [Physica B (to be published)].